J. Parasitol., 103(5), 2017, pp. 423–439

THERMAL PERFORMANCE CURVES AND THE METABOLIC THEORY OF ECOLOGY—A PRACTICAL GUIDE TO MODELS AND EXPERIMENTS FOR PARASITOLOGISTS

Péter K. Molnár, Jason P. Sckrabulis*, Karie A. Altman*, and Thomas R. Raffel*

Department of Biological Sciences, University of Toronto Scarborough, 1265 Military Trail, Toronto, Ontario, M1C 1A4, Canada. Correspondence should be sent to Péter K. Molnár at: *peter.molnar@utoronto.ca*

ABSTRACT: Climate change will affect host–parasite dynamics in complex ways. The development of forecast models is necessary for proactive disease management, but past studies have frequently reported thermal performance data in idiosyncratic ways that have limited use for parameterizing thermal host–parasite models. Development of improved forecast models will require strong collaborations between experimental parasitologists and disease modelers. The purpose of this article is to facilitate such collaborations by reviewing practical considerations for describing thermal performance curves of parasite and host performance traits, and using them to predict climate change impacts on host–parasite systems. In the first section, we provide an overview of how thermal performance curves can be embedded in life-cycle–based dynamical models of parasitism, and we outline how such models can capture the net effect of multiple nonlinear temperature dependencies affecting the host–parasite dynamics. We also discuss how macroecological generalities based on the metabolic theory of ecology (MTE) can be used to determine a priori parameter estimates for thermal performance curves to derive null models for data-deficient species, but we note that most of the generalities suggested by MTE remain to be tested for parasites. In the second section, we discuss empirical knowledge gaps for the temperature dependence of parasite and host performance traits, and we outline the types of data that need to be collected to inform MTE-based models for data-deficient species. We specifically emphasize the importance of (1) capturing the entire thermal response of performance traits, including lower and upper temperature thresholds, and (2) experimentally or statistically separating out the thermal responses of different performance traits (e.g., development and mortality) rather than only reporting composite measures (e.g., apparent development). Not adhering to these principles can lead to biased climate change impact predictions. In the third section, we provide a practical guide outlining how experimentalists can contribute to fill data gaps by measuring the temperature dependence of host and parasite performance traits in ways that are systematic, statistically rigorous, and consistent with the requirements of life cycle–based host–parasite models. This guide includes recommendations and practical examples illustrating (1) the use of perturbation analyses to determine experimental priorities, (2) experimental design tips for quantifying thermal response curves, and (3) statistical methods for estimating the parameters of thermal performance curves. Our hope is that this article helps researchers to maximize the value and use of future data collections for both empirical and modelling studies investigating the way in which temperature influences parasitism.

Temperature affects the dynamics of hosts, vectors, and parasites in multifaceted ways, with some effects benefiting parasite transmission and others acting in the opposite direction (Rogers and Randolph, 2006; Gallana et al., 2013; Raffel et al., 2013). For example, warmer temperatures typically increase the development rates of free-living parasite larvae while simultaneously reducing their survival times (Paull et al., 2012; Brady et al., 2013; Molnár et al., 2013b). Similarly, warmer temperatures generally increase the rates of development and reproduction of parasites within ectotherm hosts, but can also increase their mortality, for example, by boosting the performance of the host's immune system or by increasing natural host mortality (Raffel et al., 2006; Paull et al., 2015). Due to such interacting forces, climate change is likely to alter the phenology, ranges, and infection dynamics of hosts and parasites in complex and often nonintuitive ways (Harvell et al., 2002; Mangal et al., 2008; Pickles et al., 2013). Unraveling these complexities and forecasting likely climate change impacts on parasitism are critical to informing the management of human and wildlife diseases and remain key challenges for parasitologists and disease ecologists in the 21st century (Altizer et al., 2013).

Mathematical models provide powerful tools to synthesize multiple interacting forces and forecast short-term (weather) and long-term (climate) effects on the dynamics of hosts and parasites (Mangal et al., 2008; Pascual et al., 2008; Ewing et al., 2016; McCallum, 2016). The accuracy of such forecasts, however, is often limited by the availability of laboratory and/or field measurements showing how temperature affects key traits of host and parasite performance, that determine R_0, parasite prevalence and average abundance in hosts, and other disease metrics (Rohr et al., 2013). Such traits, collectively referred to as "performance traits" throughout this article, include physiological rates (e.g., larval development from hatching to an infective stage), vital rates (reproduction and mortality of hosts and parasites), and interaction rates between hosts and parasites (e.g., rates of parasite uptake by hosts, or host resistance to parasite establishment following uptake).

In essence, the problem is twofold. First, due to their high species diversity (Dobson et al., 2008), data only exist for a minuscule fraction of parasitic species, making it impossible to parameterize and test species-specific forecast models in most cases (Rodó et al., 2013). Second, many parasitological studies measure the temperature dependencies of performance traits in idiosyncratic ways (see section 2), making it difficult to discover among-species generalities that could inform forecast models for data-deficient species. In the absence of sufficient data or documented generalities, however, modelers must rely on untested

Received 17 October 2016; revised 11 May 2017; accepted 22 May 2017.
* Department of Biological Sciences, Oakland University, 2200 N. Squirrel Road, Rochester, Michigan 48309.
DOI: 10.1645/16-148

assumptions about the temperature dependence of model parameters, resulting in potentially unreliable model predictions and management recommendations.

This article is founded on our conviction that experimentalists and modelers need to interact more closely to maximize the value and use of parasitological data for forecasting climate effects on disease dynamics. Good parasitological data are obviously necessary for the development, parameterization, and testing of disease models; in turn, models can enhance experimental work by synthesizing diverse data in tractable frameworks, providing more sophisticated experimental predictions, and identifying key data gaps (Hilborn and Mangel, 1997; Restif et al., 2012; Urban et al., 2016). Unfortunately, this iterative process is too often hampered by poor communication between modelers and experimentalists, sometimes resulting in the collection of data that are difficult to use in the parameterization of host–parasite models (section 2). The purpose of this synthesis article is to facilitate this communication by establishing clear links among (1) life cycle–based models that characterize the impacts of temperature on host–parasite dynamics, (2) macroecological generalities based on the metabolic theory of ecology (MTE), which can inform these models, (3) parasitological data gaps that are suggested by these approaches, and (4) rigorous experimental procedures for filling these gaps. As such, our article is structured as follows:

- In section 1, we review key challenges in modeling temperature effects on the interactive dynamics of parasites and hosts, and we discuss how MTE-based life cycle models can capture the net outcome of multiple interacting temperature dependencies. To allow these models to do so, we emphasize the importance of: (1) experimentally or statistically separating out the respective temperature-dependent contributions of different performance traits to life cycle transitions (e.g., the confounding influences of larval development and mortality on the rate at which uninfective larvae reach an infective stage), and (2) capturing the entire thermal response of each performance trait, including lower and upper temperature thresholds.
- In section 2, we review the critical data and knowledge gaps that are suggested by these approaches and that currently prevent the development of reliable thermal host–parasite models for most species.
- In section 3, we provide a step-by-step guide that outlines how experimentalists can contribute to filling these gaps by measuring the temperature dependence of host and parasite performance traits in ways that are systematic, statistically rigorous, and consistent with the requirements of commonly used mechanistic host–parasite models. This guide includes recommendations and practical examples illustrating (1) the use of perturbation analyses to prioritize the performance traits that are the most critical to quantify, (2) experimental design tips for quantifying thermal response curves, and (3) best practices for the statistical analysis of thermal response data.

Throughout this article, we emphasize models of thermal performance that are based on the MTE, due to their ability to synthesize multiple thermal processes across different levels of biological organization and their potential for providing a priori parameter estimates for data-deficient species (Brown et al., 2004). We also focus primarily on parasite interactions with their hosts at the individual and population levels. However, we stress that the approaches and arguments outlined in this article are broadly applicable, including to non-MTE-based models of thermal responses, as well as for studying community-level parasite dynamics.

SECTION 1: THEORETICAL OVERVIEW

Challenges for parasite thermal biology—complex life cycles and species interactions

Most parasite life cycles include at least one environmental stage and/or a stage within an ectotherm (intermediate or definitive) host, resulting in direct temperature effects on various performance traits (Roberts et al., 2000; Rohr et al., 2011). The temperature dependencies of these traits, in turn, can interact in complex ways to influence the population dynamics of hosts and parasites, and thus also the prevalence and severity of disease (Rogers and Randolph, 2006; Gallana et al., 2013). For visualization, consider the two example life cycles in Figure 1, which we will refer to throughout this article. The first represents a nematode parasite like *Ostertagia gruehneri*, with one endotherm definitive host and a mandatory free-living stage during which larvae need to develop to infectivity (Fig. 1A, B; Molnár et al., 2013b). The second represents a two-host trematode parasite like *Schistosoma mansoni*, with one endotherm definitive host, one ectotherm intermediate host, within which both development and asexual reproduction occur, and mandatory free-living stages in between these within-host stages (Fig. 1C, D; Mangal et al., 2008).

In both examples, the host–parasite dynamics are governed by the combined influences of multiple performance traits, including physiological, vital, and interaction rates (Fig. 1B, D), and each of these traits may in turn be influenced by multiple temperature-dependent host or parasite processes (Fig. 1A, C). The probabilities of parasite establishment following infection (q_G, q_H), for example, are functions of both parasite infectivity and host resistance to infection, either one of which may be influenced by environmental temperature (Rohr et al., 2013). In general, all processes governing the host–parasite dynamics (Fig. 1; Table I) fall into one of four categories: (I) processes that occur entirely within endotherm hosts (e.g., egg production by adult parasites); (II) processes that do not involve interactions between hosts and parasites (e.g., the development rates of free-living parasite larvae or uninfected hosts); (III) host–parasite interactions before infection (encounter rates and parasite uptake); and (IV) host–parasite interactions that occur within an ectotherm host. Here, we will focus on those processes that are directly impacted by temperature (categories II–IV). The transition rates and impacts of parasites within endotherm hosts (category I) may of course also be affected by climate changes, but these effects are usually indirect, substantially more complex, and less amenable to experimentation, and they have been reviewed elsewhere (Martin et al., 2008; Morley and Lewis, 2014; Gethings et al., 2015; Mignatti et al., 2016).

Thermal performance curves and the MTE

The temperature dependence of physiological rates, vital rates, and interaction rates can be described by thermal performance curves, which display these rates as a function of temperature (Fig. 2; Angilletta, 2009). Thermal performance curves are

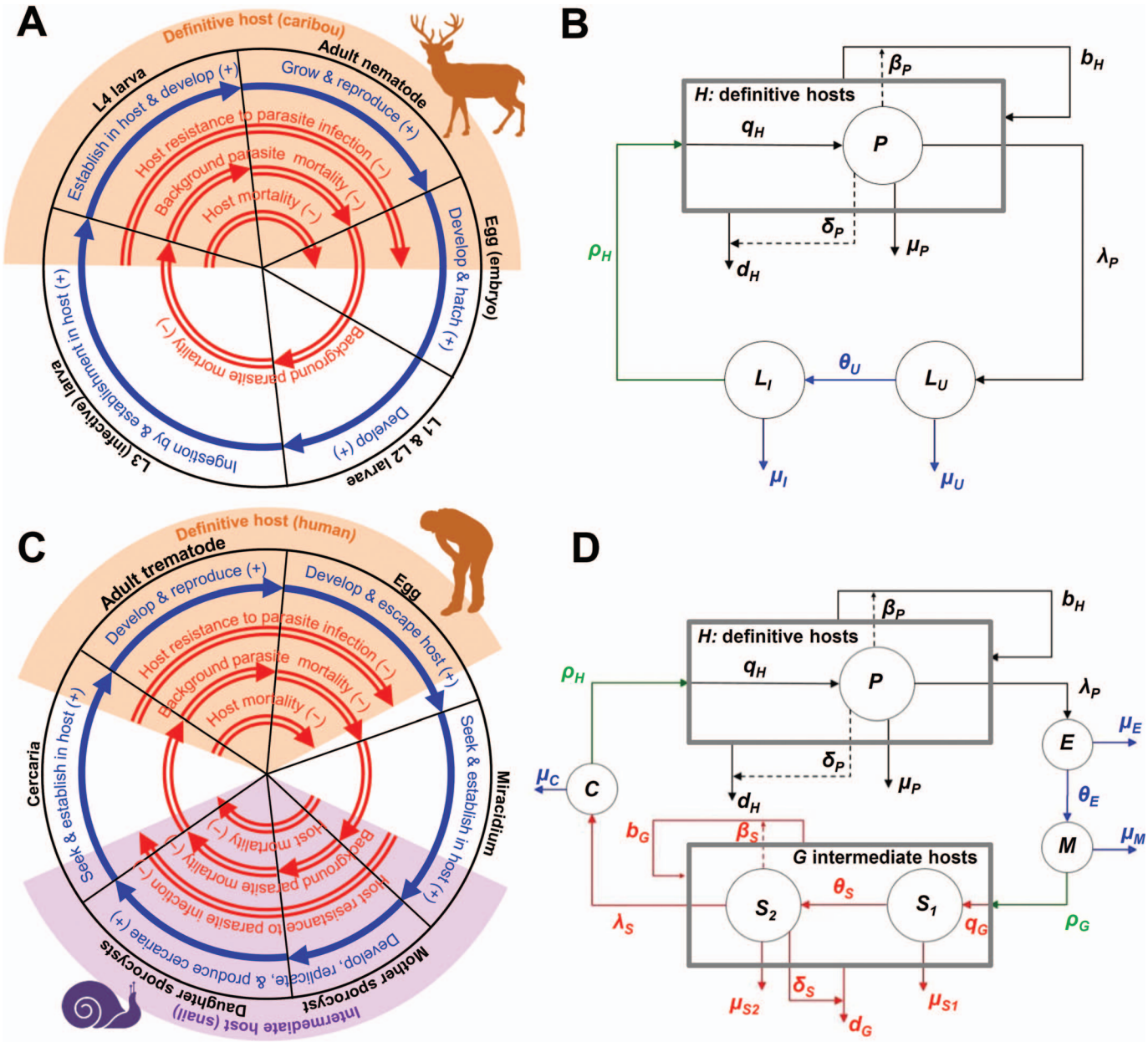

FIGURE 1. Schematic of the life cycles (**A, C**) and dynamical models (**B, D**) for two generalized parasite life cycles. A and B represent a specialist nematode with an endotherm host (H) that harbors adult parasites (P), and a mandatory free-living stage (L_U) during which larvae need to develop to infectivity (L_I). C and D represent a trematode where free-living eggs (E) hatch into miracidiae (M) that then seek out and infect intermediate hosts (G). Following establishment inside these hosts, larvae pass through multiple sporocyst stages (S_i) before they asexually produce cercariae (C) that pass out of the intermediate host and actively seek out a definitive host (H), within which they complete development to the adult stage (P). In A and C, blue and red arrows represent host or parasite performance traits that have positive and negative effects on parasite transmission, respectively. In B and D, solid arrows represent the rates of parasite birth (λ_x), development (θ_x), mortality (μ_x), and host encounter (ρ_x), the probabilities of establishment within a host following infection (q_x), as well as host birth (b_x) and death (d_x); the influences of the parasite on host birth (β_x) and death (δ_x) are marked by dashed arrows. Temperature-dependent rates and influences are marked blue for parameters that only involve a single free-living player, green for parameters that involve host–parasite interactions within the environment, and red for host–parasite interactions that occur within an ectotherm host. Parameters that are assumed to be temperature independent due to host endothermy are marked black.

TABLE I. Parameter notations for the life cycle–based host–parasite models of Figure 1, and for the underlying thermal performance curves.

Parameter	Definition	Units*
	Performance traits of hosts and parasites determining the host–parasite dynamics	
y	Metabolic rate	J · time^{-1}
λ_x	Per capita reproduction rate of stage x	Time^{-1}
θ_x	Per capita development rate of stage x	Time^{-1}
μ_x	Per capita mortality rate of stage x	Time^{-1}
ρ_x	Per capita uptake rate of parasites by host type x	Time^{-1} · host abundance^{-1}
q_x	Probability of establishment within host type x following uptake	—
b_x	Per capita rate of birth for host type x	Time^{-1}
d_x	Per capita rate of death for host type x	Time^{-1}
β_x	Instantaneous reduction in host fecundity due to the presence of parasites in stage x	Time^{-1} · parasite abundance^{-1}
δ_x	Instantaneous mortality rate of hosts due to the presence of parasites in stage x	Time^{-1} · parasite abundance^{-1}
	Parameters of thermal performance curves	
y_0, θ_0, μ_0 etc.	Baseline values of the above performance traits at a reference temperature T_0	[Units of trait] · time^{-1}
T_0	Reference temperature (set arbitrarily such that $T^L << T_0 << T^H$)	K
E_z	Activation energy of trait z	eV
E_z^L, E_z^H	Low- and high-temperature inactivation energies of trait z	eV
T_z^L, T_z^H	Low- and high-temperature inactivation thresholds for trait z	K
k	Boltzmann's constant	eV K^{-1}

* For simplicity, we report temperature values in degrees Celsius (C) throughout the manuscript; however, note that for application in the BA and SS models (equations 1, 2) these values must be transformed into Kelvin (K) by adding 273.15 degrees.

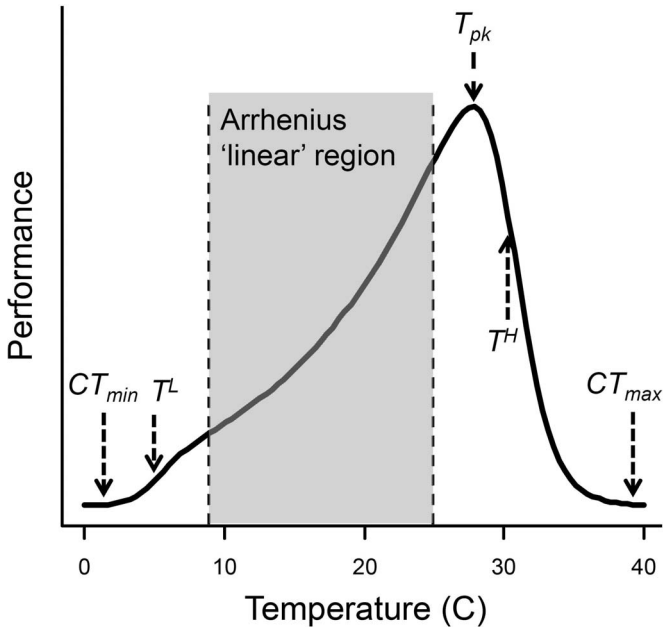

FIGURE 2. Typical thermal performance curve showing the low and high temperatures for enzyme inactivation (T^L and T^H), the temperature of peak performance (T_{pk}), the critical thermal minimum and maximum where performance drops to zero ($CT_{\min}$ and $CT_{\max}$), and the 'linear' Arrhenius region. The curve was generated using the Sharpe-Schoolfield model (equation 2) with $E = 0.65$ eV, $-E^L = E^H = 6.2$ eV, $T^L = 5$ C, and $T^H = 29$ C.

typically unimodal across all possible temperatures (i.e., exhibiting a single temperature of peak performance) and display steep threshold behavior at the lower and upper boundaries of an organism's thermal niche (Fig. 2). Various mathematical models have been developed to describe the unimodality of thermal performance curves, but most are purely phenomenological with parameters that have limited biological meaning (Régnière et al., 2012).

A mechanistic approach to describing thermal performance curves is provided by the MTE, which postulates that ecological processes across all levels of biological organization can be inferred from organismal metabolism (Brown et al., 2004), including the development, mortality, and reproduction of parasites and hosts, within-host processes such as parasite pathogenicity and host immune responses, critical disease metrics such as R_0, and community-level characteristics such as parasite biomass and abundances (Hechinger et al., 2011; Molnár et al., 2013b; Rohr et al., 2013). According to MTE, each of these processes is ultimately governed by the rates of organismal metabolism, which in turn follow predictable relationships with organism body mass and temperature (Gillooly et al., 2001, 2002). Specifically, MTE postulates that the temperature dependence of organism metabolism is governed by the reaction rates of metabolic enzymes, the activity levels of which increase exponentially as a function of temperature at intermediate temperatures of an organism's fundamental thermal niche (Gillooly et al., 2001; Brown et al., 2004; Molnár et al., 2013b). These dynamics are embodied in the Boltzmann–Arrhenius (BA) relation,

$$y(T) = y_0 e^{-\frac{E_y}{k}\left(\frac{1}{T}-\frac{1}{T_0}\right)}, \quad (1)$$

which describes metabolism, y, as a function of temperature, T (measured in Kelvin; Table I). Near the boundaries of an organism's thermal niche, where temperatures are high or low enough to reversibly inactivate key metabolic enzymes, metabolic

performance steeply drops toward zero, resulting in unimodal thermal performance curves (Sharpe and Demichele, 1977; Schoolfield et al., 1981; Dell et al., 2011; Corkrey et al., 2012; Molnár et al., 2013b). These additional dynamics are captured by a unimodal extension of the BA model, the Sharpe–Schoolfield (SS) model:

$$y(T) = y_0 e^{-\frac{E_y}{k}\left(\frac{1}{T}-\frac{1}{T_0}\right)} \cdot \left(1 + e^{\frac{E_y^L}{k}\left(\frac{1}{T_y^L}-\frac{1}{T}\right)} + e^{\frac{E_y^H}{k}\left(\frac{1}{T_y^H}-\frac{1}{T}\right)}\right)^{-1}. \quad (2)$$

In both equations, y_0 represents metabolic rate at a standardization temperature T_0, which should approximately be chosen at an intermediate value of the organism's thermal niche but can otherwise be set arbitrarily (Fig. 2; Schoolfield et al., 1981). Effects of organism size are frequently incorporated into these equations by assuming that y_0 scales allometrically with body mass (i.e., $y_0 \propto mass^{\alpha}$; Gillooly et al., 2001; Brown et al., 2004), but we will focus on the temperature-dependent components of equations 1 and 2 throughout this article. The parameter E_y represents the activation energy of the rate-limiting enzyme(s), and it describes how rapidly metabolism increases with temperature within the organism's normal tolerance range; k is Boltzmann's constant. The SS model adds realism to the BA equation by incorporating enzyme inactivation at the lower and upper temperature thresholds, T_y^L and T_y^H, with the inactivation energies E_y^L and E_y^H determining how rapidly metabolic rate rises and drops near the lower and upper boundaries of the organism's tolerance range, respectively (Table I).

Although the SS model is relatively complex, with six free parameters (y_0, E_y, T_y^L, T_y^H, E_y^L, and E_y^H), each parameter fulfills a distinct role in governing the shape of the thermal performance curve (e.g., both E_y^L and E_y^H have negligible effects at intermediate temperatures but drive performance at low and high temperature extremes, respectively). This important feature ensures parameter separability, meaning that all model parameters can be estimated when fitting the model to (sufficient) data (section 3; de Jong and van der Have, 2009; Régnière et al., 2012). Moreover, in cases where either low- or high-temperature inactivation is undetectable or irrelevant, given the temperature ranges that the parasite is or will be experiencing, equation 2 can easily be simplified to reduce the number of free parameters by removing either of these components (i.e., by setting $T_y^L = 0$ [Kelvin] or $T_y^H = \infty$; Schoolfield et al., 1981); see Suppl. Mat. Appendix S4.4 and equation S3 for an example. However, in general, we do not recommend such model reductions due to the importance of these thresholds for determining phenological changes, range changes, and the effects of increasingly frequent extreme weather events (see section 3).

From this basis, MTE derives the likely temperature dependence of higher-level biological processes by explicitly considering the relationship of each process to organismal metabolism. Processes that do not involve any species interactions (e.g., development rates or movement rates of free-living parasites; category II in the section "Challenges for parasite thermal biology-complex life cycles and species interactions"), for example, are expected to follow the BA and SS relationships with activation and inactivation energies (E_z, E_z^L, E_z^H) comparable to those of metabolism (E_y, E_y^L, E_y^H; Brown et al., 2004), but likely with a somewhat narrower thermal breadth than basal metabolism ($T_y^L < T_z^L$; $T_z^H < T_y^H$; van der Have, 2002). These expectations have been verified in a wide range of organisms and traits (Gillooly et al., 2002; Brown et al., 2004; Dell et al., 2011).

The likely temperature dependence of processes that involve species interactions (categories III and IV in the section "Challenges for parasite thermal biology-complex life cycles and species interactions") can also be described using MTE, but this requires explicit consideration of the interaction process. Survival times, for example, may relate closely to the SS model of metabolism if natural mortality outweighs predation mortality (McCoy and Gillooly, 2008; Molnár et al., 2013b), but would scale with both predator and prey metabolism otherwise (Dell et al., 2014; Gilbert et al., 2014). Similar arguments can be made for the encounter rate between parasites and hosts (category III in the section "Challenges for parasite thermal biology-complex life cycles and species interactions"), which can be derived from movement patterns and movement speeds, where the latter again tend to scale with metabolism (Pawar et al., 2012). Dell et al. (2014), for example, suggested that predator–prey encounter rates should be proportional to (1) the metabolic rate of the prey, $y_{prey}(T)$, for ambush (sit-and-wait) predation; (2) the metabolic rate of the predator, $y_{pred}(T)$, if the predator moves much faster than the prey (e.g., grazing); and (3) $\sqrt{y_{pred}(T)^2 + y_{prey}(T)^2}$ if both predator and prey move randomly at comparable speeds. [Note that in all cases, $y(T)$ is temperature independent for endotherms.] Similar relationships are likely to hold for host–parasite encounters with comparable search mechanisms, but others will require adjusting these equations to account for some of the more specialized methods of host finding (e.g., chemotaxis; Haas, 2003).

Finally, for species interactions that occur within an ectotherm host (category IV in the section "Challenges for parasite thermal biology-complex life cycles and species interactions"; Fig. 1C, D), it is again the interaction of host and parasite metabolism that determines the overall thermal performance curve. The probability of parasite establishment following uptake, as well as the rates of within-host development and reproduction (Fig. 1C, D), for example, are all expected to depend on parasite metabolism, $y_P(T)$, and should therefore increase with temperature within the parasite's thermal tolerance range. However, each of these processes may be limited by the availability of resources from the host (which typically scales with host body mass; Poulin and George-Nascimento, 2007; Hechinger, 2013; Lagrue and Poulin, 2016), and/or by the strength of the host's immune response (which typically increases with temperature and scales with host metabolism; Raffel et al., 2006; Rohr et al., 2013). As such, higher temperatures could benefit either the parasite or the host, depending on the respective strengths of these interacting processes (Rohr et al., 2013). It is thus reasonable to assume that the parasite transition rates within hosts would scale positively with $y_P(T)$, scale inversely with $y_H(T)$, and would also depend on host and parasite body mass (M_H, M_P) in nontrivial ways (Hechinger, 2013; Rohr et al., 2013; de Leo et al., 2016). Furthermore, for the same reasons, we expect similar scaling rules for the impacts of the parasite on host reproduction (β; Fig. 1D) and survival (δ; Fig. 1D), and/or for the ability of the parasite to manipulate its host (not shown in Fig. 1, but see Molnár et al., 2013a). The precise nature of these scaling rules, however, remains unclear and is an important avenue for empirical and theoretical research (see also section 2).

MTE-based biological null models for temperature effects on host–parasite dynamics

One practical benefit of the MTE approach is that it allows the development of biological null models for the overall impacts of temperature on the population- and community-level dynamics of hosts and parasites. Such null models differ from (unrealistic) null models that assume temperature has no effect on the host–parasite dynamics by (1) summarizing all life cycle transitions, vital rates, and species interactions in a dynamic host–parasite model, (2) a priori specifying the likely functional form of each thermal performance curve (see previous section), and (3) estimating unknown parameters from MTE scaling rules (see below; de Leo and Dobson, 1996; Bolzoni et al., 2008; Molnár et al., 2013b; Dobson et al., 2015). For data-deficient species, this approach can provide a first approximation of the ways in which key performance traits (e.g., development, mortality, infection), and therefore system properties (e.g., R_0, phenology, species' ranges, and the frequency of epidemic outbreaks), are expected to change with temperature changes.

For example, using an Anderson-May–type host–macroparasite model (Anderson and May, 1978) to represent the one-nematode-one-endotherm-host dynamics in Figure 1B, we obtain the following expression for R_0 (defined as the 'expected lifetime reproductive output of a newborn larva') as a function of temperature, T (see Appendix S1 for the derivation):

$$R_0(T) = C \cdot \frac{\theta_U(T)}{\mu_U(T) + \theta_U(T)} \cdot \frac{\rho_H(T)H}{\mu_I(T) + \rho_H(T)H}, \qquad (3)$$

where $C = q_H\lambda_P/(\mu_P + d_H + \delta_P)$ is a temperature-independent constant summarizing within-host processes (Fig. 1B), $\mu_U(T)$ and $\mu_I(T)$ are the stage-dependent per capita rates of larval mortality, $\theta_U(T)$ is the per capita development rate of uninfective parasite larvae to the infective stage, and $\rho_H(T)H$ is the per capita rate at which an infective larva encounters hosts (H is host abundance). Following the MTE arguments in the section "Thermal performance curves and the MTE," we can now also specify a priori expectations for the functional form of the temperature-dependent parameters $\theta_U(T)$ (SS model), $\mu_U(T)$ and $\mu_I(T)$ (variant of SS model with rates rising to infinity outside the parasite's tolerance range), and $\rho_H(T)$ (e.g., SS model for parasites that actively seek out endotherm hosts, or a temperature-independent constant for parasites that wait passively to be ingested by the host), and thus also $R_0(T)$ (equation 3; Molnár et al., 2013b).

Lastly, to fully specify the biological null model, we can use various MTE-related macroecological generalities to define a priori parameter expectations for each of the thermal performance curves [$\theta_U(T)$, $\mu_U(T)$, $\mu_I(T)$, $\rho_H(T)$] that determine $R_0(T)$. The activation energies (E), inactivation energies (E^L, E^H), and temperature thresholds (T^L, T^H) of both metabolism and derived performance traits, for example, are expected to vary systematically with covariates such as habitat, latitude, phylogenetic association, and trait function (Irlich et al., 2009; Dell et al., 2011; Sunday et al., 2011). MTE also suggests that these parameters should remain approximately invariant across different performance traits of the same organism due to their common dependence on metabolism, although this hypothesis needs further testing (Brown et al., 2004; see also section 2). Moreover, the normalization constants θ_0, μ_{U_0}, μ_{I_0}, and $\rho_{H_0}H$, representing each trait's average at a reference temperature T_0 (equations 1, 2), can potentially be estimated from allometric body mass relationships and the trophic level of parasites (Brown et al., 2004; Hechinger et al., 2011). However, most empirical MTE relationships have only been established for free-living species to date (Brown et al., 2004; McCoy and Gillooly, 2008; Dell et al., 2011; Sunday et al., 2011), so that parasitologists will initially need to refer to those studies when constructing host–parasite null models. Few data exist on the activation energies and other thermal parameters of parasites (but see Poulin, 2006; Morley, 2011, 2012), but it is our hope that this article motivates experimentalists to begin filling these gaps and deriving macroecological generalities specifically for the thermal performance of parasites (sections 2, 3).

For our example biological null model (Figs. 1B, 3; equation 3), we could estimate the normalization constants θ_0, μ_{U_0}, μ_{I_0}, and $\rho_{H_0}H$ through allometric body mass relationships. However, we will assume for the purpose of a simple example that these parameters, as well as the temperature thresholds T^L and T^H, have been previously established as $\theta_0 = 0.03$ d^{-1}, $\mu_{U_0} = \mu_{I_0} = 0.06$ d^{-1}, and $\rho_{H_0}H = 0.01$ d^{-1}, with $T_0 = 22.5$ C, $T^L = 10$ C, and $T^H = 35$ C. Furthermore, we assume that no other information exists on the temperature dependence of development, mortality, or infection, so we set the unknown activation and inactivation energies of all three traits to the approximate interspecific means of free-living species, $E = 0.65$ eV, $E^L = -5 \times 0.65$ eV $= -3.25$ eV, and $E^H = 5 \times 0.65$ eV $= 3.25$ eV (Molnár et al., 2013b). {For this, it should be noted that some publications (e.g., Kooijman, 2010; Molnár et al., 2013b) report positive rather than negative values of E^L, but that this is only due to the use of a version of the SS model where the sign of the term $\exp[E_y{}^L/k(1/T_y{}^L - 1/T)]$ in equation 2 is reversed (i.e., $\exp[E_y{}^L/k(-1/T_y{}^L + 1/T)]$, rather than due to biological variation in the low-temperature inactivation energy.} The resulting expected temperature dependency of $R_0(T)$ (Fig. 3) is of course fraught with large uncertainties and has limited predictive capability. Nevertheless, such biological null models can provide initial rules of thumb for expected climate change impacts on understudied and newly emerging parasites, and they can provide guidance to researchers regarding the system components that are the most critical to understand for improving the accuracy of climate change predictions (see section 3). Targeting these sensitive parameters in subsequent laboratory and/or field experiments can then iteratively improve the model to obtain increasingly accurate species-specific forecasts (Restif et al., 2012; Urban et al., 2016).

Contrasting the MTE approach and linear degree-day models: key differences

One main reason for estimating thermal performance curves and synthesizing this information in host–parasite models is to predict the impacts of climate warming on host–parasite systems. To accomplish this, the MTE approach emphasizes (1) a clear separation of mechanisms both at the trait level (development, mortality, etc.) and at the underlying physiological level (activation and inactivation energies, etc.); (2) the synthesis of these mechanisms in dynamical host–parasite models to capture the net effect of multiple positive and negative temperature dependencies; and (3) the importance of capturing the nonlinearity of thermal performance curves across the organism's entire thermal niche. An alternative approach that is frequently used to describe thermal performance and to infer potential climate

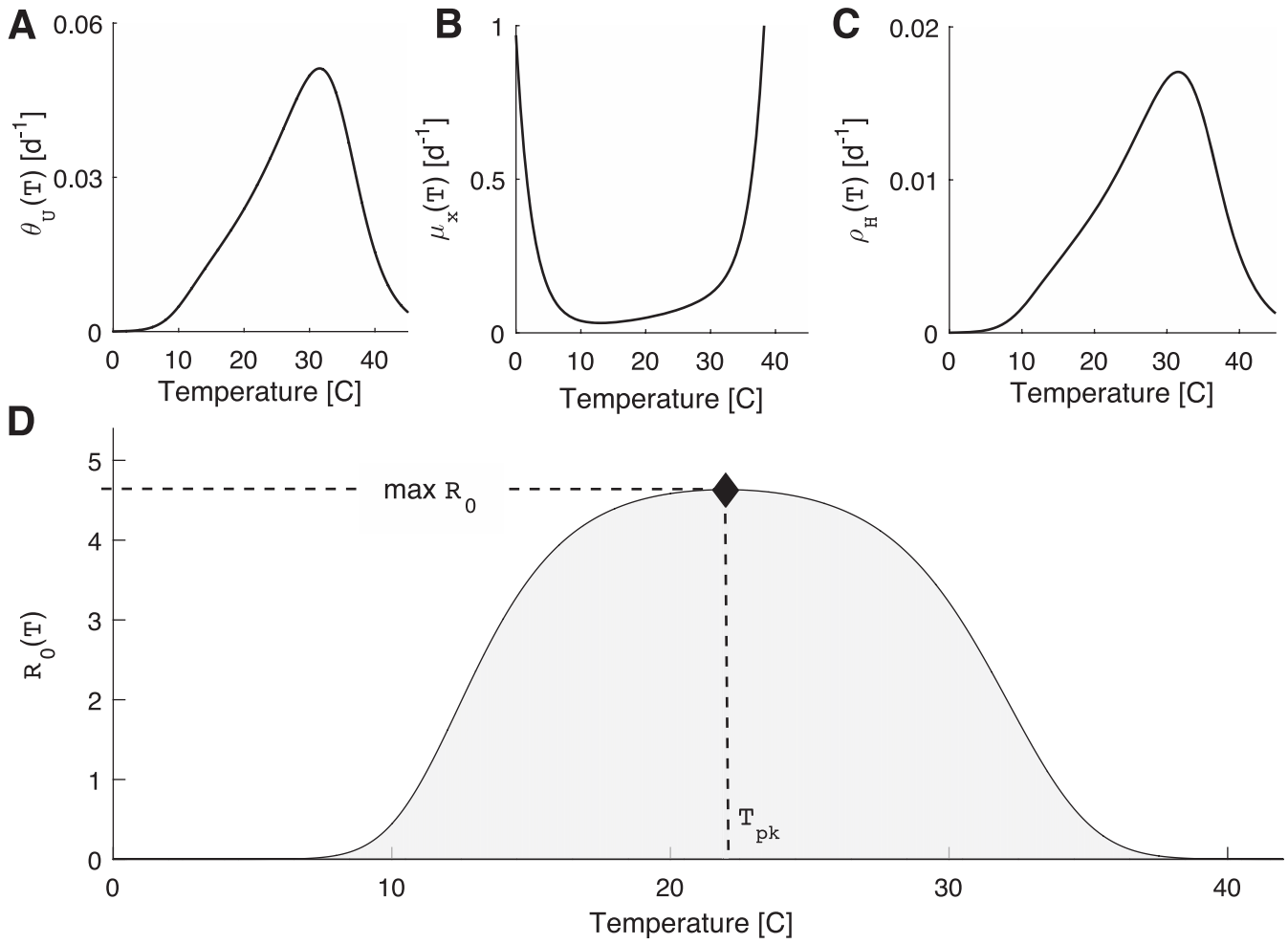

FIGURE 3. Biological null model for the temperature-dependent basic reproductive number $R_0(T)$ of a specialist nematode with an endotherm definitive host, a mandatory free-living stage during which larvae need to develop to infectivity, and active infection. (**A–C**) Null models for the underlying temperature dependency of free-living larval development (θ_U), mortality (μ_U, μ_I), and host encounter (ρ_H). (**D**) Resultant null model for $R_0(T)$ (equation 3), with a diamond marking the temperature T_{pk} at which $R_0(T)$ is maximized, and the area-under-the-curve AUC($R_0(T)$) shaded gray (see section 3; Fig. 4). Note that $R_0(T)$ is symmetric despite the asymmetric shape of its underlying components, $\theta_U(T)$, $\mu_U(T)$, $\mu_I(T)$, and $\rho_H(T)$, because the temperature dependencies of the positive (development, host encounter) and negative (mortality) influences on $R_0(T)$ cancel each other out at intermediate temperatures under the null assumption of equal activation energies, inactivation energies, and temperature thresholds for development, mortality, and encounter rates (see equation 3).

change impacts, but which does not adhere to the above principles, is to use a linear degree-day model. In this section, we highlight the consequences of these differences, and refer the reader to Moore and Remais (2014) for a general discussion on the limitations of degree-day models.

Like the BA and SS models, degree-day models aim to describe the thermal dependence of performance traits. However, in contrast to the MTE-based approaches, degree-day models assume a linear relationship between performance and temperature (T), and they are typically formulated only for a subset of the life cycle processes that determine the host–parasite dynamics (e.g., just for larval development, θ, but ignoring mortality effects, μ_x):

$$\theta(T) = \begin{cases} DD^{-1}(T - CT_{\min}) & \text{for } CT_{\min} < T < T_{\max} \\ 0 & \text{otherwise} \end{cases}, \quad (4)$$

where the parameter DD (the inverse of the slope) can be interpreted as the number of degree-days required to complete development, $CT_{\min}$ is the minimum temperature needed for development, and $T_{\max}$ is an upper temperature threshold set below $CT_{\max}$ to avoid overestimating development at high temperatures (Trudgill et al., 2005; Moore and Remais, 2014). Once parameterized, degree-day models are typically used to estimate whether a parasite could complete one or more life cycle stages in a given location under various climate scenarios, now or in the future (Kutz et al., 2005; Zhou et al., 2008; McCreesh and Booth, 2013), by integrating equation 4 over the temperatures experienced by the parasite in that location.

The validity of this approach depends on a variety of questionable assumptions (Moore and Remais, 2014), and in particular on the degree to which the linear model in equation 4 approximates the inherently nonlinear temperature dependence of organism performance. At intermediate temperatures, this approximation can be fairly accurate (but see, e.g., Kilpatrick et al., 2008), perhaps because the exponential Arrhenius relationship is somewhat linearized by enzyme inactivation near the lower and

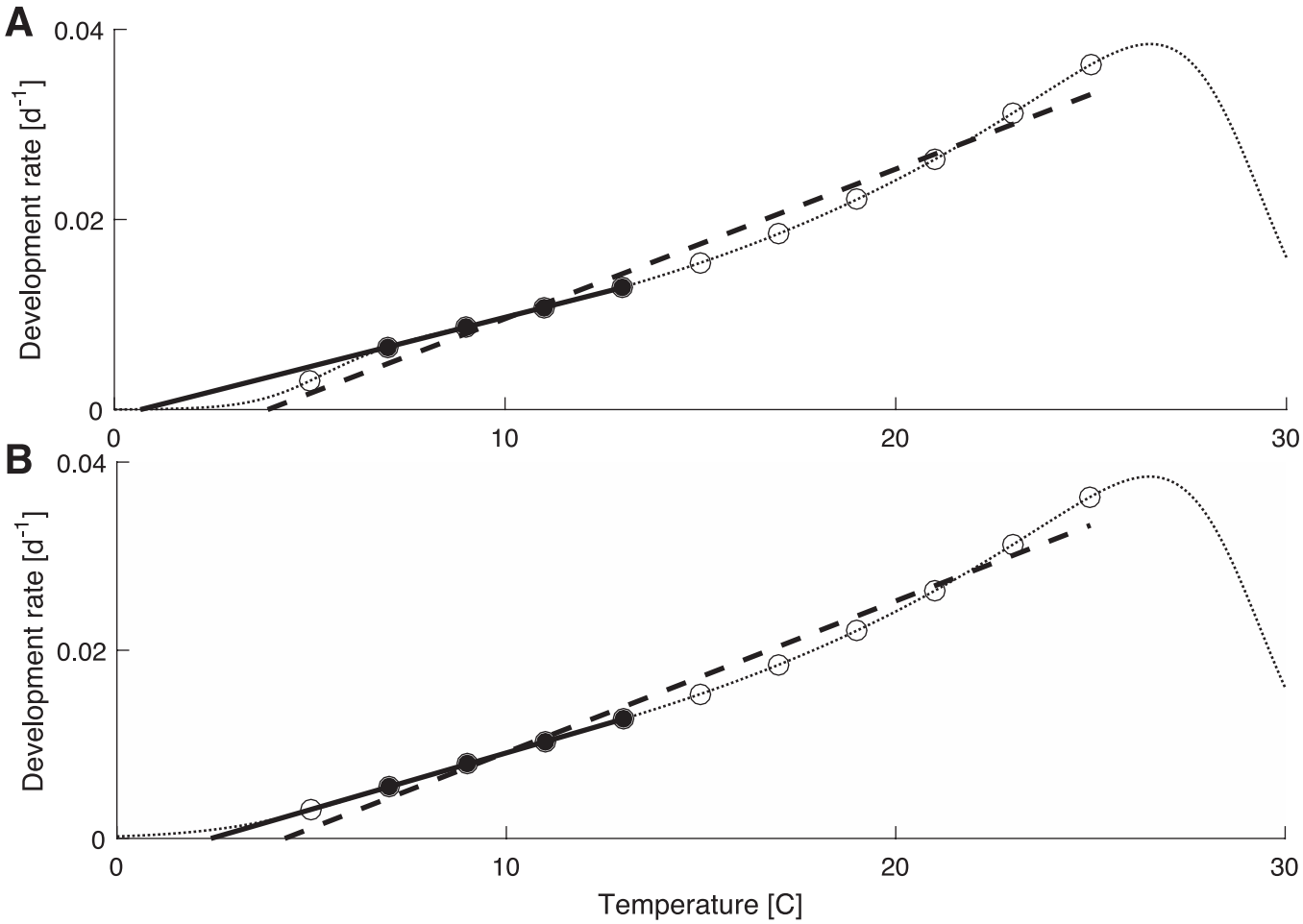

FIGURE 4. Linear degree-day models may overestimate or underestimate the minimum temperature at which development is possible. To illustrate this, we simulated a nonlinear thermal performance curve of development (dotted line), using the Sharpe-Schoolfield model with parameters $\theta_0 = 0.03$ d^{-1} (at $T_0 = 24.5$ C), $E = 0.65$ eV, $E^H = 7.3$ eV, $T^L = 5$ C, $T^H = 29$ C, and low-temperature inactivation energies $E^L = -7.3$ eV (**A**) and $E^L = -3.15$ eV (**B**). We then assume that Researcher 1 collected development rate data from 5 C ($=T^L$) up to 25 C at a 2 C resolution (filled and open circles), and that Researcher 2 collected data only at 7, 9, 11, and 13 C (filled circles only). We further assume that neither researcher employed transfer experiments to measure the extremely slow development below $T^L = 5$ C. Rather, linear (degree-day) models were fit to estimate the minimum temperature at which development becomes impossible, $CT_{\min}$ (dashed and solid lines). Such extrapolations can over- or underestimate $CT_{\min}$ depending on the range of temperatures for which data are available (A), and the steepness of the inactivation drop-off near T^L (contrast solid lines in A and B).

upper thermal thresholds (Fig. 2; Charnov and Gillooly, 2003; Trudgill et al., 2005). However, this assumption becomes problematic at temperatures near $CT_{\min}$, especially when $CT_{\min}$ is estimated by linear extrapolation from the apparently linear relation at intermediate temperatures, as is commonly done (Trudgill et al., 2005). Such extrapolations may overestimate or underestimate the true $CT_{\min}$, depending on the temperature range of the available data (Moore and Remais, 2014; Pawar et al., 2016) and the true value of the inactivation energy E^L, which determines the degree of nonlinearity at low temperature extremes (Fig. 4). Similar issues arise in the choice of $T_{\max}$, which can only crudely approximate the effects of high-temperature inactivation (Moore and Remais, 2014). However, accurate threshold estimates are critical for predicting changes in phenology and range (Molnár et al., 2013b) and the effects of increasingly frequent extreme temperature events (Vasseur et al., 2014). As such, we recommend characterizing the entire thermal performance curve of traits by using transfer experiments to capture low performance at temperature extremes (section 3; Régnière et al., 2012), rather than relying on a linear approximation of a nonlinear process that can result in threshold biases in unknown directions.

Moreover, we caution that degree-day models are usually limited to a subset of the processes determining the host–parasite dynamics, rendering them uninformative regarding climate change impacts at the population level. A developmental degree-day model, for example, may indicate a substantially decreased development time for nematode eggs to reach the infective L3 stage at increased temperatures (Jenkins et al., 2006; Kutz et al., 2013), but the resulting benefits for the parasite could easily be negated by increased mortality during development or at the L3 stage (Fig. 3; equation 3). Whether a temperature change causes a decrease or increase in R_0 (or other disease metrics) can therefore only be unraveled with an approach that considers the entire life cycle (cf. above), and not by models that omit parts of the life cycle. The predictions of developmental degree-day models should thus be interpreted with extreme

caution and at best be considered an index for potential climate change impacts.

SECTION 2: DATA GAPS

Comprehensive temperature profiles that include all or most performance traits that influence the host–parasite dynamics can be used for forecasting range changes and other changes to the host–parasite dynamics (Ryan et al., 2015; Rose et al., 2016), but exist only for a few select diseases, such as malaria (Mordecai et al., 2013) or Lyme disease (Ostfeld and Brunner, 2015). For some others, thermal performance has been quantified for parts of the parasite's thermal niche (e.g., excluding thresholds) and/or for parts of its life cycle (e.g., development only), but detailed quantitative information is lacking for the vast majority of species. Developing a comprehensive thermal database for parasites will be challenging, but the MTE approach suggests guidelines for how to fill existing data gaps in systematic ways that maximize information, both for species-specific and for broad-scale interspecific predictions.

First, the MTE suggests that the activation and inactivation energies of metabolism (y) and metabolism-dependent traits (e.g., development, θ; mortality, μ; movement speed, v) should be approximately similar in a given individual (e.g., $E_y \approx E_\theta \approx E_\mu \approx E_v$; Brown et al., 2004). However, this is almost certainly an overly simplistic assumption, because different physiological processes are likely accomplished by different suites of potentially rate-limiting enzymes, in addition to the shared suite of metabolic enzymes (Seebacher et al., 2003; Trudgill et al., 2005). Indeed, there is evidence that activation energies vary according to the physiological function of a particular process (Dell et al., 2011). Determining the cases in which the MTE assumption of equal activation energies across metabolically dependent traits within a given individual holds true, and whether deviations are systematic and can be predicted from covariates, would radically simplify data needs. As such, metabolic data should be collected alongside the thermal performance curves of different traits, taking care to separate out individual contributions to composite terms (e.g., parasite establishment as a composite of parasite infectivity and host resistance to infection; see section 2) to ensure valid among-trait comparisons. Deviations from the BA and SS models are also possible (e.g., thermostable zones where performance does not vary with temperature; Morley, 2012) and should be carefully documented to determine how often, in what direction, and under what conditions such deviations should be expected.

Second, the MTE suggests that within- and among-species variation in activation energies, inactivation energies, and temperature thresholds of thermal performance curves might be predictable from variables such as habitat, latitude, and phylogenetic association (Irlich et al., 2009; Munch and Salinas, 2009; Dell et al., 2011; Sunday et al., 2011; Nilsson-Ortman et al., 2013; Pawar et al., 2016). In free-living species, such relationships are well documented and have been used to derive broad-scale predictions for climate change impacts on unicellular organisms, insects, reptiles, and amphibians (Deutsch et al., 2008; Dillon et al., 2010). Some indication exists for similar relationships in parasites (e.g., latitudinal trends in the temperature sensitivity of trematode infectivity and cercaria emergence; Poulin, 2006; Morley and Lewis, 2015). However, broader systematic analyses are lacking, largely because of insufficient data coverage. Similarly, it is unclear how and to what extent mass scaling laws can be used to accurately estimate normalization constants of parasite performance (y_0 in equations 1 and 2), and in particular whether the metabolic rates of internal parasites should scale with parasite mass, host mass, or some combination of these (Hechinger, 2013; de Leo et al., 2016). We recommend that parasitologists systematically select representative species to broaden the coverage of latitudes, habitats, and other covariates that may influence thermal performance to establish macro-ecological generalities like those found in free-living species.

Third, the MTE also provides possible solutions for modeling complex biological responses to temperature variability. For example, organisms often exhibit thermal acclimation responses following a temperature shift, resulting in altered thermal performance curves (Angilletta, 2009; Dowd et al., 2015). MTE suggests that parasites might generally have faster acclimation responses than their hosts due to their smaller size, which might give parasites an advantage over their hosts in variable-temperature conditions (Raffel et al., 2013; Rohr et al., 2013). Such acclimation effects can be incorporated into the BA or SS models by allowing key parameters like E and T^H to vary as functions of the organism's acclimation temperature (Rohr et al., 2013). Moreover, many organisms, including parasites, also possess adaptive responses to predictable diurnal or seasonal shifts in temperature (Martinez-Bakker and Helm, 2015), and these complexities might potentially be described using similar model extensions. However, we currently lack data on the rate, magnitude, and nature of thermal acclimation responses for most parasites (but see Altman et al., 2016), and more will be needed before we can test for systematic patterns.

Lastly, we note that much of the data that currently exist on the thermal performance of parasites have been reported in idiosyncratic ways, making interspecific comparisons difficult. Development time, for example, has been reported as 'time when the first larva of an experimentally reared cohort reached a target stage' or as the 'time when 50% [or some other percentage] of the cohort reached that stage' (e.g., Young et al., 1980; Kutz et al., 2001). More fundamentally, many studies report *apparent* development times (i.e., the development time distribution of those individuals that lived long enough to complete development), sometimes augmented by information on *apparent* mortality (i.e., the percentage of individuals that completed development; Gibson, 1981; van Dijk and Morgan, 2011). Other studies have estimated the real development time and mortality rate distributions (i.e., including those individuals that die before completing development) by statistically disentangling these rates from the time series of cohort development/mortality (e.g., Smith, 1990). These approaches are neither equivalent nor will they lead to comparable estimates of temperature sensitivity, because both apparent development and apparent mortality are in reality composite measures of the real rates of development and mortality (Braner and Hairston, 1989). As a consequence, apparent development times will typically be more temperature sensitive (higher E) than real development times, while apparent mortality (as defined above) will typically be less temperature sensitive than the real mortality rate (Fig. 5; Appendix S2). Similar issues are likely to arise for any composite measure of a life cycle transition. For example, parasite establishment (i.e., the 'proportion of parasites that establish within a host') is sometimes interpreted as a measure of parasite performance and sometimes

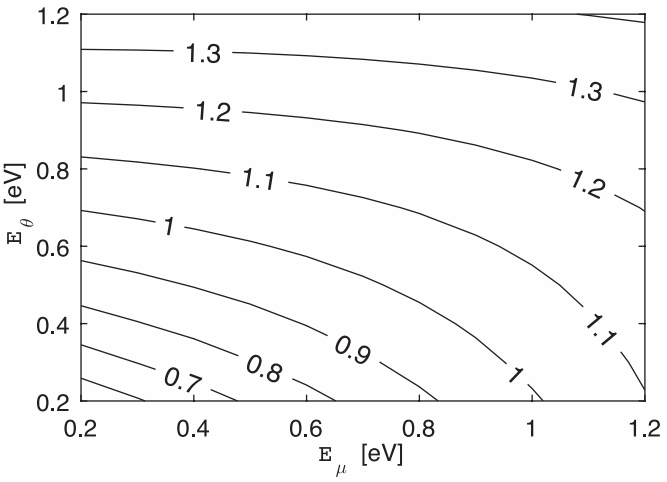

FIGURE 5. Contour lines showing the apparent activation energy of development (E_θ') that would be estimated for different combinations of the true activation energy of development (E_θ) and the activation energy of mortality (E_μ) if the influence of mortality is not correctly separated out. Note that the apparent activation energy of development E_θ' consistently overestimates the true activation energy E_θ. Results were derived following the model of Braner and Hairston (1989), assuming normally distributed development times with a temperature-dependent mean, $M(T)$, that is described by the BA equation (equation 1) and a temperature-independent variance σ^2 around this mean, as well as a temperature-dependent mortality rate $\mu(T)$ that is also described by the BA equation. Parameter values are $M(T_0) = 10$ d, $\mu_0(T_0) = 0.5$ d^{-1}, $T_0 = 20$ C, and $\sigma^2 = 10$ d^2. For discussion of the underlying mechanisms causing these patterns, see Appendix S2.

as a measure of host resistance, whereas in reality it is a composite metric influenced by both parasite infectivity and host resistance to infection (Rohr et al., 2013). Misinterpreting the thermal response of composite parameters as the thermal response of a single mechanism can substantially bias climate change impact predictions (Fig. 5). To avoid such issues and ensure comparability between different studies, we recommend statistically separating composite processes where possible (see also section 3), and reporting the full empirical distribution (means, variances, skewness, etc.) for each process (e.g., development and mortality; parasite infectivity and host resistance; etc.) and all temperature treatments. In contrast to composite parameters, the resulting thermal performance curves can be input into dynamic host–parasite models in a straightforward manner (Fig. 1).

SECTION 3: A PRACTICAL GUIDE

Here we provide guidelines for collecting high-quality thermal performance data on the life cycle of parasites, including how to decide which performance traits to prioritize for measurement, experimental design tips, and analytical methods for fitting the BA and SS models to data.

Deciding which performance traits to prioritize (perturbation analyses)

Because the overall impacts of climate change on parasitism depend on multiple interacting nonlinear thermal performance curves (Figs. 1, 3), it is generally advisable to measure the thermal responses of as many life cycle transition rates, vital rates, and interaction traits as possible for a given species of interest (sections 1, 2). However, funding and logistical constraints force most researchers to prioritize experiments and decide a priori the traits on which to focus. One strategy to setting such research priorities is to first develop a biological null model for the overall host–parasite dynamics that is parameterized with literature estimates for known parameters and using MTE scaling rules for unknown parameters (section 1). Perturbation analyses (i.e., sensitivity or elasticity analyses) can then inform the researcher about the traits that are likely to have the greatest effects on the temperature dependence of the host–parasite dynamics and should therefore be targeted in experiments (Urban et al., 2016).

The main difficulty with the perturbation analysis of temperature-dependent host–parasite dynamics is that the respective importance of different traits may vary between temperatures (Fig. S2). The classical approach to such perturbation analyses therefore determines the additive contribution of each trait to the temperature sensitivity of $R_0(T)$, dR_0/dT, separately for each possible temperature, using the chain rule of derivation (Fig. S2; Rogers and Randolph, 2006; Mordecai et al., 2013). While this approach can be extended to calculate the additive contributions of each trait's underlying thermal parameters (y_0, E, E^L, E^H, T_0, T^L, T^H; equation 2) to dR_0/dT, such analyses become difficult to interpret with a large number of traits and parameters. We therefore suggest an alternative approach that summarizes key properties of $R_0(T)$ in two numerical values that are amenable to the simpler methods of scalar perturbation analysis (de Kroon et al., 2000; Caswell, 2001).

First, we consider the area-under-the-curve of $R_0(T)$ (Fig. 3)

$$\mathrm{AUC}\big(R_0(T)\big) = \int_0^\infty R_0(T)dT, \tag{5a}$$

which is proportional to the average parasite R_0 across all possible temperatures (note that temperature is measured in Kelvin, which is why the integration limit starts at zero).

Second, we consider the skewness of $R_0(T)$, which determines whether R_0 peaks at a relatively high (left-skewed), intermediate (bell-shaped), or low (right-skewed) temperature within the parasite's thermal niche. This skewness is not only a key determinant of how performance varies among individuals in a stochastic environment (Dowd et al., 2015), but it also determines whether infection risk will likely increase or decrease in different parts of a parasite's geographic range with climate change (Altizer et al., 2013; Molnár et al., 2013b). With malaria, for example, some studies suggested a left-skewed $R_0(T)$ that peaks at about 31 C, while others suggested a bell-shaped $R_0(T)$ peaking at about 25 C (Mordecai et al., 2013). The consequences of these differences are dramatic, as a 31 C peak implies an increased infection risk across almost all of the parasite's current range with climate change, whereas a 25 C peak implies a decreased infection risk in many areas that will be getting too hot for the parasite to survive (Altizer et al., 2013; Mordecai et al., 2013). As such, we define the metric

$$s\big(R_0(T)\big) = \frac{T_{pk} - T^L}{T^H - T^L}, \tag{5b}$$

which shows the relation of the temperature where $R_0(T)$ is maximized (T_{pk}) to the (known or assumed) lower and upper temperature thresholds T^L and T^H, with $s < 0.5$ indicating right-

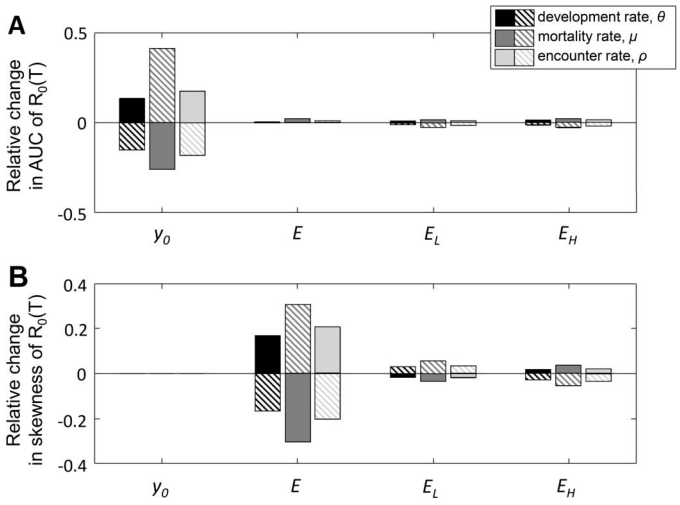

FIGURE 6. Perturbation analysis of an MTE-parameterized biological null model for a nematode with an endotherm host, a mandatory free-living stage, and active host infection. Baseline parameters of development (θ), mortality (μ), and encounter (ρ) rates are set as $\theta_0 = 0.03$ d^{-1}, $\mu_0 = 0.06$ d^{-1}, $\rho_0 = 0.01$ d^{-1} at $T_0 = 22.5$ C, and as $E = 0.65$ eV, $-E^L = E^H = 3.25$ eV, $T^L = 10$ C, $T^H = 35$ C for all three traits; see section 3 for details. The elasticities of (**A**) the area-under-the-curve of $R_0(T)$ and (**B**) the skewness measure $s(R_0(T))$ (equation 5) are shown with respect to the normalization constant (y_0), activation energies (E), and the low- and high-temperature inactivation energies (E^L, E^H) of development (black), mortality (dark gray), and host encounter (light gray). The effect of a 20% increase (solid) or decrease (hatched) is shown for each parameter.

skewed $R_0(T)$, and $s > 0.5$ indicating left-skewed $R_0(T)$. We then calculate how both AUC($R_0(T)$) and $s(R_0(T))$ change in response to a proportional change in any of the model parameters that determine the temperature sensitivity of the underlying performance traits. Formally, this approach is known as an elasticity analysis (de Kroon et al., 2000).

Suppose, for example, we are interested in studying the thermal dynamics of an environmentally transmitted nematode with an endotherm definitive host (e.g., Fig. 1A, B), for which the thermal performance thresholds of free-living larvae ($T^L = 10$ C, $T^H = 35$ C) and their rates of development, mortality, and infection ($\theta_0 = 0.03$ d^{-1}, $\mu_0 = 0.06$ d^{-1}, $\rho_0 = 0.01$ d^{-1}, respectively) at a reference temperature ($T_0 = 22.5$ C) are approximately known. However, no information exists on the temperature sensitivity (i.e., the activation and inactivation energies) of these traits. A biological null model that incorporates these knowns and unknowns can then be obtained by specifying thermal performance curves for development, mortality, and infection as outlined in section 1, fixing known parameters (θ_0, μ_0, ρ_0, T_0, T^L, T^H) to their measured values, setting all activation and inactivation energies to their interspecific means ($E = 0.65$ eV, $-E^L = E^H = 3.25$ eV; Fig. 3), and embedding these curves in an appropriate model of the host–parasite dynamics. Here, we illustrate this approach using the ordinary differential equation framework of Anderson and May (1978) to represent the host–parasite dynamics (see section 1; Fig. 3). However, note that researchers should in general explore several alternative model structures (e.g., inclusion of developmental delays, or increased resolution of life stages by explicitly including the L1, L2, L3 stages, etc.) to ensure that the conclusions regarding research priorities are unaffected by uncertainties about model structure (Babtie et al., 2014).

Both the classical approach and our suggested approach show that larval mortality is the most critical parameter influencing the thermal dynamics of this parasite, followed by host infection and development (Figs. 6, S2; see Appendix S3 for the corresponding R-codes). In addition, we observe that the baseline values θ_0, μ_0, and ρ_0 are by far the most critical influence on AUC($R_0(T)$) (Fig. 6A), whereas the activation energies E_θ, E_μ, and E_ρ determine changes in the skewness of $R_0(T)$ (Fig. 6B; see also Molnár et al., 2013b). The inactivation energies, by contrast, have relatively small effects on either metric (Fig. 6). Understanding the temperature dependence of mortality, and specifically μ_0 and E_μ, should therefore be prioritized in this particular system. Once these parameters are determined accurately, these perturbation analyses should be repeated to determine the next priority, as the ranking of parameter elasticities might change as parameter values get updated (de Kroon et al., 2000).

For more complex life cycles, such perturbation analyses would proceed in an analogous way and could further be augmented by elasticity loop analyses (de Kroon et al., 2000), which can be used to determine the most critical life cycle paths and hosts in parasites that can use two or more alternative paths (hosts) to complete their life cycles (e.g., alternative mammalian hosts for *Schistosoma mansoni*; Fig. 1C). Similarly, researchers may be interested in more complex effects of climate change (e.g., phenology and range changes), in which case more complex null models or objective functions (e.g., incorporating seasonal or spatial dynamics) might be required. However, regardless of complexity, the same principles remain, allowing researchers to use a priori perturbation analyses to determine maximally informative research directions.

Experimental design considerations

Selecting temperature treatments: One of the most critical decisions is the choice of an appropriate number and range of temperature treatments. The activation energy E of a thermal performance curve, for example, can theoretically be estimated from a minimum of four distinct temperature treatments, located within the intermediate thermal range of the organism (i.e., between T^L and T^H), using the BA model (equation 1). However, such estimates are usually fraught with inaccuracy and imprecision, and they may also be systematically biased if some temperature treatments are inadvertently chosen too close to T^L or T^H (Fig. 7A; Pawar et al., 2016). Indeed, it is possible to obtain unrealistic negative estimates of E if all or most of the selected temperature treatments are above T_{pk} (Figs. 2, 7A). To avoid these issues, and because of the importance of temperature thresholds in determining range changes and other climate change impacts (Deutsch et al., 2008), we instead recommend characterizing the full thermal performance curve where feasible. In cases where this is not feasible, we suggest following the experimental design recommendations of Pawar et al. (2016, p. E50) to minimize biases and maximize precision. As thermal performance is driven by different parameters in the lower (E^L, T^L), intermediate (E, y_0), and upper (E^H, T^H) ranges of the parasite's thermal niche (equation 2), we recommend sampling at least four distinct temperatures in each of these three regions (12 temperatures total) for full characterization of a thermal performance curve. Smaller numbers of temperature treatments might be sufficient to characterize a partial thermal performance

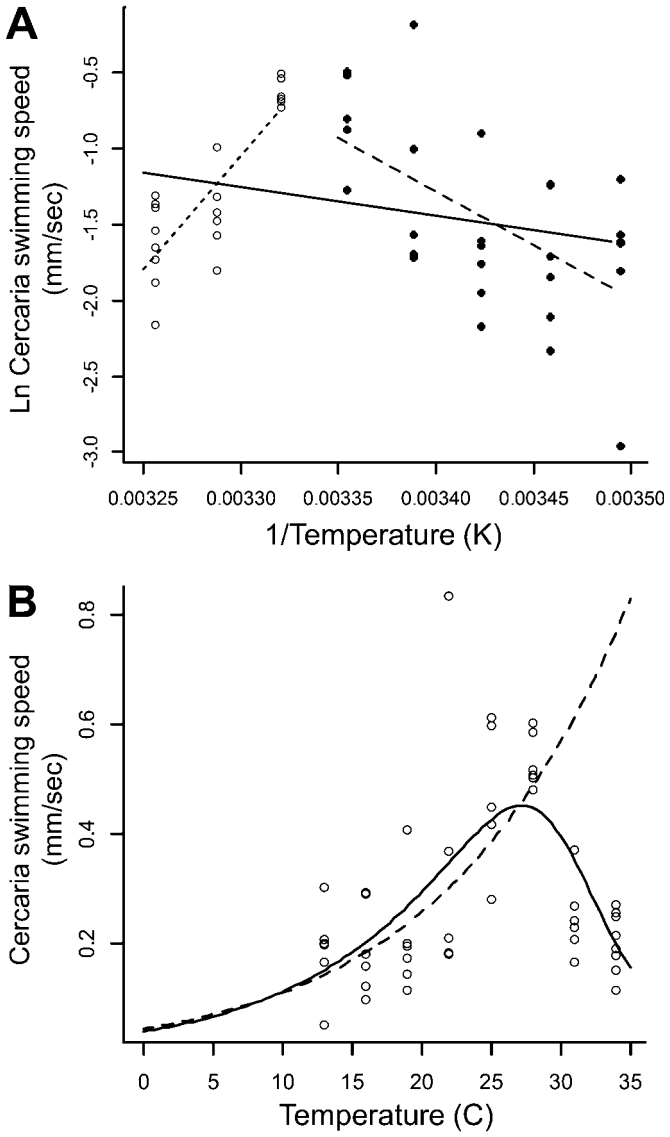

FIGURE 7. Performance curve model fits to *Schistosoma mansoni* cercaria swimming speed data. (**A**) Log-transformed *S. mansoni* cercaria swimming speed data, with the BA model once fit only to data below T_{pk} (13–25 C; filled circles and dashed line; $E = 0.608$ eV), once fit only to data above T_{pk} (28–34 C; open circles and dotted line; $E = -1.291$ eV), and once fit to the full data set (13–34 C; filled and open circles, solid line; $E = 0.162$ eV). The latter two BA model fits underestimate the activation energy E due to influence of high-temperature inactivation, illustrating the importance of selecting appropriate temperature treatments and the potential to obtain unrealistic negative estimates of E (cf. section 3; Pawar et al., 2016). (**B**) Comparison of the BA model (fit to only the lower temperatures, 13–25 C; dashed line; $E = 0.608$ eV), and the Sharpe-Schoolfield model (fit to the full data set, solid line; $E = 0.698$ eV). Note that the activation energy estimates are similar but nonetheless differ due to the additional information used in the fit of the SS model.

curve (e.g., Fig. 7B), but this might make it impossible to estimate some SS model parameters (e.g., T^L and E^L in our empirical example; Appendix S4). One benefit of this sampling strategy is that its high resolution near the lower and upper temperature thresholds T^L and T^H allows the (potentially steep) performance drop-offs caused by E^L and E^H to be captured. If T^L and T^H are unknown, pilot studies and/or literature comparisons with related species should be used to determine appropriate sampling regions a priori. By definition, T^L and T^H are generally close to, but a few degrees higher or lower than, an organism's critical thermal minimum ($CT_{\min}$) or maximum ($CT_{\max}$), respectively (van der Have, 2002).

In addition to these fixed-temperature treatments, we also recommend transfer experiments where the organism is exposed to two or more temperature treatments successively (e.g., Régnière et al., 2012; Altman et al., 2016). Such experiments can approximate the effects of natural temperature variability and can, for example, be used to estimate thermal acclimation responses (Raffel et al., 2013; Altman et al., 2016). Moreover, transfer experiments can help estimate parameters that might otherwise be obscured by high mortality (Régnière et al., 2012). For example, Régnière et al. (2012) found that larval development was difficult to measure at temperatures near T^H because larvae died before they could complete development. They solved this problem by starting larvae at the high target temperature, before transferring them to a temperature well below T^H. This allowed completion of development but at a faster overall rate than would be expected for the low-temperature treatment due to the high-temperature head start (Régnière et al., 2012). Teasing apart such contributions is critical for estimating parasite performance under variable temperatures, and in particular, for understanding the likely impacts of increasingly frequent extreme weather events (Kutz et al., 2009; Vasseur et al., 2014).

Avoiding pseudoreplication: Logistical and other limitations usually require a trade-off between the number of distinct temperature treatments and the number of replicates per treatment in an experiment. Due to the importance of selecting as many temperature treatments as possible (see above), we recommend prioritizing the former if necessary but still suggest including at least two true replicates per temperature treatment to guard against random events skewing results, especially near T^L and T^H, where strong nonlinearities and increased among-individual variance might affect the accuracy and precision of estimates.

True replication of temperature treatments can be challenging when, for example, only a few incubators are available. One solution to this dilemma is to increase replication by conducting measurements in multiple temporal blocks, with each incubator randomly assigned to a new temperature treatment in subsequent blocks (e.g., Altman et al., 2016). This strategy can be particularly effective when measurements can be obtained quickly (e.g., metabolism, respiration, muscle performance) but poses a challenge for measuring host or parasite performance traits that need to be measured over extended time periods (e.g., rates of development or infection). One solution in this latter case is to purchase or construct multiple low-cost incubators to obtain sufficient replication in a single temporal block (Raffel et al., 2013; Greenspan et al., 2016). One can also improve the precision of parameter estimates by testing multiple organisms in each incubator simultaneously, and then account for pseudo-

replication post-hoc by including 'incubator' as a random effect in subsequent analyses (e.g., Altman et al., 2016).

Individual- vs. cohort-based sampling to quantify waiting-time processes: Many performance traits are waiting-time processes, such as 'time to complete development' or 'time to mortality.' The associated rates for these processes (e.g., θ_U and μ_U in Fig. 1B) are best estimated from time-to-occurrence data from individual parasites followed over time ('individual-based sampling'). However, it is often more convenient to raise parasites as groups ('cohort-based sampling'), which typically results in so-called stage-frequency data (the proportions of parasites in different life stages, such as developmental stages, as a function of time; e.g., Young et al., 1980; Kutz et al., 2001). If only a single process is studied, such as the natural mortality of free-living nondeveloping parasite stages (e.g., nematode L3, or trematode miracidia and cercariae; Fig. 1), mortality rates can be estimated from either cohort or individual data using standard survival analyses (Lebreton et al., 1993). However, most life cycle transitions involve multiple simultaneous processes that cannot be studied in isolation from one another (Fig. 1). As outlined in section 2, failure to disentangle composite processes can lead to systematic biases when estimating the thermal sensitivity of host and parasite performance traits (Fig. 5). While advanced statistical methods are available to disentangle multiple simultaneous processes from cohort-based stage-frequency data (e.g., Manly, 1990; de Valpine and Knape, 2015), loss of information and increased model complexity lower the precision and accuracy of parameter estimates (Régnière et al., 2012). In contrast, individual-based sampling makes it relatively simple to separate interacting processes like parasite development versus mortality or parasite infectivity versus host resistance, leading to improved parameter estimates (Régnière et al., 2012). We therefore recommend an individual-based sampling approach whenever practicable, and post-hoc statistical separation of composite processes from stage-frequency data when cohort-based sampling must be employed.

Fitting the BA and SS models to thermal performance data

The parameters of the SS model can be determined by fitting the model to thermal performance data using maximum likelihood techniques (Xiao et al., 2011; Régnière et al., 2012). Similar to traditional nonlinear least-squares regression, maximum likelihood seeks to find those parameter values that maximize model fit to the data. However, in contrast to least-squares regression (which implicitly assumes a normally distributed error), maximum likelihood allows flexibility regarding the error distribution of the data (Hilborn and Mangel, 1997). Régnière and Powell (2003) argued that the error distribution of thermal performance data (expressed as 'observed/expected') should generally be lognormal because (normally distributed) biological parameters (e.g., the activation energy E) appear within exponential terms in the BA and SS models. Following these arguments, Régnière et al. (2012) developed a formal likelihood approach for estimating the parameters of the SS model, which we illustrate in Appendix S4 using an example data set from *Schistosoma mansoni* cercaria swimming speeds across eight temperatures (Fig. 7B). To aid other researchers, we also provide the R code used in this example for parameter estimation, as well as example code that allows for the addition of potential random effects in the sampling design (e.g., populations raised in multiple incubators; Appendix S4). However, we also note that these likelihood functions and the corresponding codes may have to be adjusted to the specifics of an experiment, for example, to account for noncontinuous observations in long-running experiments (Régnière et al., 2012) or for error distributions that are not lognormal (Xiao et al., 2011).

In situations where the data are restricted to the 'linear' portion of the thermal performance curve (Fig. 2), the activation energy E can still be estimated by fitting the log-transformed BA model to log-transformed performance data using linear regression (Fig. 7A). As with the above outlined likelihood approach for the SS model, this approach implicitly assumes a lognormal error distribution (as opposed to a nonlinear least-squares regression on untransformed data), and it should be ensured that this error distribution matches the error structure of the data (Xiao et al., 2011). Moreover, it is critical that only data points from within the 'linear' portion of the thermal performance curve are included when fitting the BA model, because the nonlinearity operating at low and high temperatures may bias activation energy estimates otherwise (Fig. 7A; Pawar et al., 2016).

CONCLUSIONS

Most researchers studying climate impacts on parasites are focused on generating predictions for one or a few specific target species. The guidelines we suggest herein will help increase the accuracy and power of such predictions. They will also ensure a minimum level of standardization to facilitate interspecific comparisons and the development of biological null models for data-deficient species. We fully expect that some species and patterns will not conform to current MTE expectations, and parasites in particular have a unique lifestyle that might lead to interesting deviations (Hechinger et al., 2011). However, it is such exceptions that lead to the modification of current paradigms (del Rio, 2008). Ultimately, the data must decide whether the thermal performance of hosts and parasites is most appropriately described by the SS and/or BA models, and any significant deviations should be documented carefully to inform the next generation of thermal host–parasite models. Nevertheless, the MTE provides a pragmatic way forward for improving both our theoretical understanding of the thermal biology of parasitism and our ability to predict climate impacts on specific target species.

ACKNOWLEDGMENTS

We would like to thank J. Koprivnikar for organizing the ASP symposium that precipitated this paper. We would also like to thank M. L. Messner and L. Shamoun for assisting with video analysis of *Schistosoma mansoni* swimming speed, and J. S. Vargas Soto for translating our Matlab code for the perturbation analyses into R scripts. *Biomphalaria glabrata* M-line snails exposed to *S. mansoni* parasites were provided by the Schistosome Research Reagent Resource Center for distribution by BEI Resources, NIAID, NIH: NR-21961. Work by P.K.M. was funded by ArcticNet, the Networks of Centres of Excellence of Canada, and a Natural Sciences and Engineering Research Council of Canada Discovery Grant. Work by T.R.R., J.P.S., and K.A.A. was funded by an NSF grant (IOS 1121529) and

internal awards from the Oakland University Research Excellence Fund and University Research Committee.

LITERATURE CITED

ALTIZER, S., R. S. OSTFELD, P. T. J. JOHNSON, S. KUTZ, AND C. D. HARVELL. 2013. Climate change and infectious diseases: FROM evidence to a predictive framework. Science **341:** 514–519.

ALTMAN, K. A., S. H. PAULL, P. T. JOHNSON, M. N. GOLEMBIESKI, J. P. STEPHENS, B. E. LAFONTE, AND T. R. RAFFEL. 2016. Host and parasite thermal acclimation responses depend on the stage of infection. Journal of Animal Ecology **85:** 1014–1024.

ANDERSON, R. M., AND R. M. MAY. 1978. Regulation and stability of host–parasite population interactions: I. Regulatory processes. Journal of Animal Ecology **47:** 219–247.

ANGILLETTA, M. J. 2009. Thermal adaptation: a theoretical and empirical synthesis. Oxford University Press, Cambridge, U.K., 320 p.

BABTIE, A. C., P. KIRK, AND M. P. H. STUMPF. 2014. Topological sensitivity analysis for systems biology. Proceedings of the National Academy of Sciences of the United States of America **111:** 18507–18512.

BOLZONI, L., A. P. DOBSON, M. GATTO, AND G. A. DE LEO. 2008. Allometric scaling and seasonality in the epidemics of wildlife diseases. American Naturalist **172:** 818–828.

BRADY, O. J., M. A. JOHANSSON, C. A. GUERRA, S. BHATT, N. GOLDING, D. M. PIGOTT, H. DELATTE, M. G. GRECH, P. T. LEISNHAM, R. MACIEL-DE-FREITAS, ET AL. 2013. Modelling adult *Aedes aegypti* and *Aedes albopictus* survival at different temperatures in laboratory and field settings. Parasites & Vectors **6:** 351.

BRANER, M., AND N. G. HAIRSTON. 1989. From cohort data to life table parameters via stochastic modeling. *In* Estimation and analysis of insect populations, L. L. McDonald, B. F. J. Manly, J. A. Lockwood, and J. A. Logan (eds.). Springer-Verlag, Berlin, Germany, p. 81–92.

BROWN, J. H., J. F. GILLOOLY, A. P. ALLEN, V. M. SAVAGE, AND G. B. WEST. 2004. Toward a metabolic theory of ecology. Ecology **85:** 1771–1789.

CASWELL, H. 2001. Matrix population models: construction, analysis and interpretation, 2nd ed. Sinauer, Sunderland, Massachusetts, 722 p.

CHARNOV, E. L., AND J. F. GILLOOLY. 2003. Thermal time: body size, food quality and the 10 degrees C rule. Evolutionary Ecology Research **5:** 43–51.

CORKREY, R., J. OLLEY, D. RATKOWSKY, T. MCMEEKIN, AND T. ROSS. 2012. Universality of thermodynamic constants governing biological growth rates. Plos One **7:** e32003.

DE JONG, G., AND T. M. VAN DER HAVE. 2009. Temperature dependence of development rate, growth rate and size: from biophysics to adaptation. *In* Phenotypic plasticity of insects: mechanisms and consequences, D. W. Whitman, and T. N. Ananthakrishnan (eds.). CRC Press, Boca Raton, Florida, p. 461–526.

DE KROON, H., J. VAN GROENENDAEL, AND J. EHRLEN. 2000. Elasticities: a review of methods and model limitations. Ecology **81:** 607–618.

DE LEO, G. A., AND A. P. DOBSON. 1996. Allometry and simple epidemic models for microparasites. Nature **379:** 720–722.

DE LEO, G. A., A. P. DOBSON, AND M. GATTO. 2016. Body size and meta-community structure: the allometric scaling of parasitic worm communities in their mammalian hosts. Parasitology **143:** 880–893.

DE VALPINE, P., AND J. KNAPE. 2015. Estimation of general multistage models from cohort data. Journal of Agricultural, Biological and Environmental Statistics **20:** 140–155.

DEL RIO, M. C. 2008. Metabolic theory or metabolic models? Trends in Ecology & Evolution **23:** 256–260.

DELL, A. I., S. PAWAR, AND V. SAVAGE. 2011. Systematic variation in the temperature dependence of physiological and ecological traits. Proceedings of the National Academy of Sciences of the United States of America **108:** 10591–10596.

DELL, A. I., S. PAWAR, AND V. SAVAGE. 2014. Temperature dependence of trophic interactions are driven by asymmetry of species responses and foraging strategy. Journal of Animal Ecology **83:** 70–84.

DEUTSCH, C. A., J. J. TEWKSBURY, R. B. HUEY, K. S. SHELDON, C. K. GHALAMBOR, D. C. HAAK, AND P. R. MARTIN. 2008. Impacts of climate warming on terrestrial ectotherms across latitude. Proceedings of the National Academy of Sciences of the United States of America **105:** 6668–6672.

DILLON, M. E., G. WANG, AND R. B. HUEY. 2010. Global metabolic impacts of recent climate warming. Nature **467:** 704–788.

DOBSON, A., K. D. LAFFERTY, A. M. KURIS, R. F. HECHINGER, AND W. JETZ. 2008. Homage to Linnaeus: How many parasites? How many hosts? Proceedings of the National Academy of Sciences of the United States of America **105:** 11482–11489.

DOBSON, A., P. K. MOLNÁR, AND S. KUTZ. 2015. Climate change and Arctic parasites. Trends in Parasitology **31:** 181–188.

DOWD, W. W., F. A. KING, AND M. W. DENNY. 2015. Thermal variation, thermal extremes and the physiological performance of individuals. Journal of Experimental Biology **218:** 1956–1967.

EWING, D. A., C. A. COBBOLD, B. V. PURSE, M. A. NUNN, AND S. M. WHITE. 2016. Modelling the effect of temperature on the seasonal population dynamics of temperate mosquitoes. Journal of Theoretical Biology **400:** 65–79.

GALLANA, M., M. P. RYSER-DEGIORGIS, T. WAHLI, AND H. SEGNER. 2013. Climate change and infectious diseases of wildlife: Altered interactions between pathogens, vectors and hosts. Current Zoology **59:** 427–437.

GETHINGS, O. J., H. ROSE, S. MITCHELL, J. VAN DIJK, AND E. R. MORGAN. 2015. Asynchrony in host and parasite phenology may decrease disease risk in livestock under climate warming: *Nematodirus battus* in lambs as a case study. Parasitology **142:** 1306–1317.

GIBSON, M. 1981. The effect of constant and changing temperatures on the development rates of the eggs and larvae of *Ostertagia ostertagi*. Journal of Thermal Biology **6:** 389–394.

GILBERT, B., T. D. TUNNEY, K. S. MCCANN, J. P. DELONG, D. A. VASSEUR, V. SAVAGE, J. B. SHURIN, A. I. DELL, B. T. BARTON, C. D. G. HARLEY, ET AL. 2014. A bioenergetic framework for the temperature dependence of trophic interactions. Ecology Letters **17:** 902–914.

GILLOOLY, J. F., J. H. BROWN, G. B. WEST, V. M. SAVAGE, AND E. L. CHARNOV. 2001. Effects of size and temperature on metabolic rate. Science **293:** 2248–2251.

Gillooly, J. F., E. L. Charnov, G. B. West, V. M. Savage, and J. H. Brown. 2002. Effects of size and temperature on developmental time. Nature **417:** 70–73.

Greenspan, S. E., W. Morris, R. Warburton, L. Edwards, R. Duffy, D. A. Pike, L. Schwarzkopf, and R. A. Alford. 2016. Low-cost fluctuating-temperature chamber for experimental ecology. Methods in Ecology and Evolution **7:** 1567–1574.

Haas, W. 2003. Parasitic worms: strategies of host finding, recognition and invasion. Zoology **106:** 349–364.

Harvell, C. D., C. E. Mitchell, J. R. Ward, S. Altizer, A. P. Dobson, R. S. Ostfeld, and M. D. Samuel. 2002. Climate warming and disease risks for terrestrial and marine biota. Science **296:** 2158–2162.

Hechinger, R. F. 2013. A metabolic and body-size scaling framework for parasite within-host abundance, biomass, and energy flux. American Naturalist **182:** 234–248.

Hechinger, R. F., K. D. Lafferty, A. P. Dobson, J. H. Brown, and A. M. Kuris. 2011. A common scaling rule for abundance, energetics, and production of parasitic and free-living species. Science **333:** 445–448.

Hilborn, R., and M. Mangel. 1997. The ecological detective: confronting models with data. Princeton University Press, Princeton, New Jersey, 336 p.

Irlich, U. M., J. S. Terblanche, T. M. Blackburn, and S. L. Chown. 2009. Insect rate–temperature relationships: environmental variation and the metabolic theory of ecology. American Naturalist **174:** 819–835.

Jenkins, E. J., A. M. Veitch, S. J. Kutz, E. P. Hoberg, and L. Polley. 2006. Climate change and the epidemiology of protostrongylid nematodes in northern ecosystems: *Parelaphostrongylus odocoilei* and *Protostrongylus stilesi* in Dall's sheep (*Ovis d. dalli*). Parasitology **132:** 387–401.

Kilpatrick, A. M., M. A. Meola, R. M. Moudy, and L. D. Kramer. 2008. Temperature, viral genetics, and the transmission of West Nile virus by *Culex pipiens* mosquitoes. Plos Pathogens **4:** e1000092.

Kooijman, S. A. L. M. 2010. Dynamic energy budget theory for metabolic organization, 3rd ed. Cambridge University Press, Cambridge, U.K., 532 p.

Kutz, S. J., S. Checkley, G. G. Verocai, M. Dumond, E. P. Hoberg, R. Peacock, J. P. Wu, K. Orsel, K. Seegers, A. L. Warren, et al. 2013. Invasion, establishment, and range expansion of two parasitic nematodes in the Canadian Arctic. Global Change Biology **19:** 3254–3262.

Kutz, S. J., E. P. Hoberg, and L. Polley. 2001. *Umingmakstrongylus pallikuukensis* (Nematoda: Protostrongylidae) in gastropods: larval morphology, morphometrics, and development rates. Journal of Parasitology **87:** 527–535.

Kutz, S. J., E. P. Hoberg, L. Polley, and E. J. Jenkins. 2005. Global warming is changing the dynamics of Arctic host–parasite systems. Proceedings of the Royal Society B–Biological Sciences **272:** 2571–2576.

Kutz, S. J., E. J. Jenkins, A. M. Veitch, J. Ducrocq, L. Polley, B. Elkin, and S. Lair. 2009. The Arctic as a model for anticipating, preventing, and mitigating climate change impacts on host–parasite interactions. Veterinary Parasitology **163:** 217–228.

Lagrue, C., and R. Poulin. 2016. The scaling of parasite biomass with host biomass in lake ecosystems: are parasites limited by host resources? Ecography **39:** 507–514.

Lebreton, J. D., R. Pradel, and J. Clobert. 1993. The statistical analysis of survival in animal populations. Trends in Ecology & Evolution **8:** 91–95.

Mangal, T. D., S. Paterson, and A. Fenton. 2008. Predicting the impact of long-term temperature changes on the epidemiology and control of schistosomiasis: a mechanistic model. Plos One **3:** e1438.

Manly, B. F. J. 1990. Stage-structured populations: sampling, analysis and simulation. Chapman and Hall, London, U.K., 187 p.

Martin, L. B., Z. M. Weil, and R. J. Nelson. 2008. Seasonal changes in vertebrate immune activity: mediation by physiological trade-offs. Philosophical Transactions of the Royal Society B–Biological Sciences **363:** 321–339.

Martinez-Bakker, M., and B. Helm. 2015. The influence of biological rhythms on host–parasite interactions. Trends in Ecology & Evolution **30:** 314–326.

McCallum, H. 2016. Models for managing wildlife disease. Parasitology **143:** 805–820.

McCoy, M. W., and J. F. Gillooly. 2008. Predicting natural mortality rates of plants and animals. Ecology Letters **11:** 710–716.

McCreesh, N., and M. Booth. 2013. Challenges in predicting the effects of climate change on *Schistosoma mansoni* and *Schistosoma haematobium* transmission potential. Trends in Parasitology **29:** 548–555.

Mignatti, A., B. Boag, and I. M. Cattadori. 2016. Host immunity shapes the impact of climate changes on the dynamics of parasite infections. Proceedings of the National Academy of Sciences of the United States of America **113:** 2970–2975.

Molnár, P. K., A. P. Dobson and S. J. Kutz. 2013a. Gimme shelter—the relative sensitivity of parasitic nematodes with direct and indirect life cycles to climate change. Global Change Biology **19:** 3291–3305.

Molnár, P. K., S. J. Kutz, B. M. Hoar, and A. P. Dobson. 2013b. Metabolic approaches to understanding climate change impacts on seasonal host–macroparasite dynamics. Ecology Letters **16:** 9–21.

Moore, J. L., and J. V. Remais. 2014. Developmental models for estimating ecological responses to environmental variability: structural, parametric, and experimental issues. Acta Biotheoretica **62:** 69–90.

Mordecai, E. A., K. P. Paaijmans, L. R. Johnson, C. Balzer, T. Ben-Horin, E. Moor, A. McNally, S. Pawar, S. J. Ryan, T. C. Smith, et al. 2013. Optimal temperature for malaria transmission is dramatically lower than previously predicted. Ecology Letters **16:** 22–30.

Morley, N. J. 2011. Thermodynamics of cercarial survival and metabolism in a changing climate. Parasitology **138:** 1442–1452.

Morley, N. J. 2012. Thermodynamics of miracidial survival and metabolism. Parasitology **139:** 1640–1651.

Morley, N. J., and J. W. Lewis. 2014. Temperature stress and parasitism of endothermic hosts under climate change. Trends in Parasitology **30:** 221–227.

Morley, N. J., and J. W. Lewis. 2015. Thermodynamics of trematode infectivity. Parasitology **142:** 585–597.

Munch, S. B., and S. Salinas. 2009. Latitudinal variation in lifespan within species is explained by the metabolic theory of

ecology. Proceedings of the National Academy of Sciences of the United States of America **106:** 13860–13864.

Nilsson-Ortman, V., R. Stoks, M. De Block, and F. Johansson. 2013. Latitudinal patterns of phenology and age-specific thermal performance across six *Coenagrion* damselfly species. Ecological Monographs **83:** 491–510.

Ostfeld, R. S., and J. L. Brunner. 2015. Climate change and *Ixodes* tick-borne diseases of humans. Philosophical Transactions of the Royal Society B–Biological Sciences **370:** 20140051.

Pascual, M., L. F. Chaves, B. Cash, X. Rodo, and M. Yunus. 2008. Predicting endemic cholera: the role of climate variability and disease dynamics. Climate Research **36:** 131–140.

Paull, S. H., B. E. LaFonte, and P. T. J. Johnson. 2012. Temperature-driven shifts in a host–parasite interaction drive nonlinear changes in disease risk. Global Change Biology **18:** 3558–3567.

Paull, S. H., T. R. Raffel, B. E. LaFonte, and P. T. J. Johnson. 2015. How temperature shifts affect parasite production: testing the roles of thermal stress and acclimation. Functional Ecology **29:** 941–950.

Pawar, S., A. I. Dell, and V. Savage. 2012. Dimensionality of consumer search space drives trophic interaction strengths. Nature **486:** 485–489.

Pawar, S., A. I. Dell, V. M. Savage, and J. L. Knies. 2016. Real versus artificial variation in the thermal sensitivity of biological traits. American Naturalist **187:** E41–E52.

Pickles, R. S. A., D. Thornton, R. Feldman, A. Marques, and D. L. Murray. 2013. Predicting shifts in parasite distribution with climate change: a multitrophic level approach. Global Change Biology **19:** 2645–2654.

Poulin, R. 2006. Global warming and temperature-mediated increases in cercarial emergence in trematode parasites. Parasitology **132:** 143–151.

Poulin, R., and M. George-Nascimento. 2007. The scaling of total parasite biomass with host body mass. International Journal for Parasitology **37:** 359–364.

Raffel, T. R., J. R. Rohr, J. M. Kiesecker, and P. J. Hudson. 2006. Negative effects of changing temperature on amphibian immunity under field conditions. Functional Ecology **20:** 819–828.

Raffel, T. R., J. M. Romansic, N. T. Halstead, T. A. McMahon, M. D. Venesky, and J. R. Rohr. 2013. Disease and thermal acclimation in a more variable and unpredictable climate. Nature Climate Change **3:** 146–151.

Régnière, J., and J. Powell. 2003. Animal life cycle models. *In* Phenology: an integrative environmental science, M. D. Schwarz (ed.). Springer, Berlin, Germany, p. 295–315.

Régnière, J., J. Powell, B. Bentz, and V. Nealis. 2012. Effects of temperature on development, survival and reproduction of insects: experimental design, data analysis and modeling. Journal of Insect Physiology **58:** 634–647.

Restif, O., D. T. Hayman, J. R. Pulliam, R. K. Plowright, D. B. George, A. D. Luis, A. A. Cunningham, R. A. Bowen, A. R. Fooks, T. J. O'Shea, et al. 2012. Model-guided fieldwork: practical guidelines for multidisciplinary research on wildlife ecological and epidemiological dynamics. Ecology Letters **15:** 1083–1094.

Roberts, L. S., J. Janovy Jr., and S. Nadler. 2000. Gerald D. Schmidt & Larry S. Roberts' foundations of parasitology, 9th ed. McGraw-Hill, New York, New York, 670 p.

Rodó, X., M. Pascual, F. J. Doblas-Reyes, A. Gershunov, D. A. Stone, F. Giorgi, P. J. Hudson, J. Kinter, M. A. Rodriguez-Arias, N. C. Stenseth, et al. 2013. Climate change and infectious diseases: can we meet the needs for better prediction? Climatic Change **118:** 625–640.

Rogers, D. J., and S. E. Randolph. 2006. Climate change and vector-borne diseases. Advances in Parasitology **62:** 345–381.

Rohr, J. R., A. P. Dobson, P. T. J. Johnson, A. M. Kilpatrick, S. H. Paull, T. R. Raffel, D. Ruiz-Moreno, and M. B. Thomas. 2011. Frontiers in climate change-disease research. Trends in Ecology & Evolution **26:** 270–277.

Rohr, J. R., T. R. Raffel, A. R. Blaustein, P. T. J. Johnson, S. H. Paull, and S. Young. 2013. Using physiology to understand climate-driven changes in disease and their implications for conservation. Conservation Physiology **1:** 1–15.

Rose, H., C. Caminade, M. B. Bolajoko, P. Phelan, J. van Dijk, M. Baylis, D. Williams, and E. R. Morgan. 2016. Climate-driven changes to the spatio-temporal distribution of the parasitic nematode, *Haemonchus contortus*, in sheep in Europe. Global Chang Biology **22:** 1271–1285.

Ryan, S. J., A. McNally, L. R. Johnson, E. A. Mordecai, T. Ben-Horin, K. Paaijmans, and K. D. Lafferty. 2015. Mapping physiological suitability limits for malaria in Africa under climate change. Vector-Borne and Zoonotic Diseases **15:** 718–725.

Schoolfield, R. M., P. J. H. Sharpe, and C. E. Magnuson. 1981. Non-linear regression of biological temperature-dependent rate models based on absolute reaction-rate theory. Journal of Theoretical Biology **88:** 719–731.

Seebacher, F., H. Guderley, R. M. Elsey, and P. L. Trosclair. 2003. Seasonal acclimatisation of muscle metabolic enzymes in a reptile (*Alligator mississippiensis*). Journal of Experimental Biology **206:** 1193–1200.

Sharpe, P. J. H., and D. W. Demichele. 1977. Reaction-kinetics of poikilotherm development. Journal of Theoretical Biology **64:** 649–670.

Smith, G. 1990. The population biology of the free-living phase of *Haemonchus contortus*. Parasitology **101:** 309–316.

Sunday, J. M., A. E. Bates, and N. K. Dulvy. 2011. Global analysis of thermal tolerance and latitude in ectotherms. Proceedings of the Royal Society B–Biological Sciences **278:** 1823–1830.

Trudgill, D. L., A. Honek, D. Li, and N. M. Van Straalen. 2005. Thermal time—concepts and utility. Annals of Applied Biology **146:** 1–14.

Urban, M. C., G. Bocedi, A. P. Hendry, J. B. Mihoub, G. Pe'er, A. Singer, J. R. Bridle, L. G. Crozier, L. De Meester, W. Godsoe, et al. 2016. Improving the forecast for biodiversity under climate change. Science **353:** aad8466.

van der Have, T. M. 2002. A proximate model for thermal tolerance in ectotherms. Oikos **98:** 141–155.

van Dijk, J., and E. R. Morgan. 2011. The influence of water on the migration of infective trichostrongyloid larvae onto grass. Parasitology **138:** 780–788.

Vasseur, D. A., J. P. DeLong, B. Gilbert, H. S. Greig, C. D. G. Harley, K. S. McCann, V. Savage, T. D. Tunney, and M. I.

O'Connor. 2014. Increased temperature variation poses a greater risk to species than climate warming. Proceedings of the Royal Society B–Biological Sciences **281:** 20132612.

Xiao, X., E. P. White, M. B. Hooten, and S. L. Durham. 2011. On the use of log-transformation vs. nonlinear regression for analyzing biological power laws. Ecology **92:** 1887–1894.

Young, R. R., R. M. Nicholson, R. L. Tweedie, and H. J. Schuh. 1980. Quantitative modelling and prediction of development times of the free-living stages of *Ostertagia ostertagi* under controlled and field conditions. Parasitology **81:** 493–505.

Zhou, X. N., G. J. Yang, K. Yang, X. H. Wang, Q. B. Hong, L. P. Sun, J. B. Malone, T. K. Kristensen, N. R. Bergquist, and J. Utzinger. 2008. Potential impact of climate change on schistosomiasis transmission in China. American Journal of Tropical Medicine and Hygiene **78:** 188–194.

Supporting Information

for

Thermal performance curves and the Metabolic Theory of Ecology – a practical guide to models and experiments for parasitologists

Péter K. Molnár, Jason P. Sckrabulis, Karie A. Altman, Thomas R. Raffel

CONTENT:

Appendix S1. Anderson-May-type model for the host-parasite dynamics of a one-nematode-one-endotherm-host system (Fig. 1B).

In this Appendix, we specify a dynamic host-parasite model for the one-nematode-one-endotherm-host dynamics shown in Figure 1B. Here, adult parasites reside within the endotherm host and produce transmission stages that pass out of the host into the environment. Free-living larvae then need to pass through one or more developmental stages before they become infective and can be taken up again by the host. All transition rates may hereby depend on temperature if they occur outside the definitive host, but are assumed temperature-independent otherwise due to host endothermy (Fig. 1B). Following the classical framework of Anderson & May, we obtain a set of coupled differential equations that explicitly track the abundance of hosts, (H), adult parasites within hosts (P), and free-living uninfective (L_U) and infective (L_I) larvae as a function of temperature (T) through time (t) (Anderson & May, 1978; Molnár et al., 2013);

(S1a) $$\frac{dL_U}{dt} = \lambda_P P - \mu_U(T)L_U - \theta_U(T)L_U$$

(S1b) $$\frac{dL_I}{dt} = \theta_U(T)L_U - \mu_I(T)L_I - \rho_H(T)HL_I,$$

(S1c) $$\frac{dP}{dt} = q_H \rho_H(T)HL_I - (\mu_P + d_H)P - \delta_P H\left(\frac{P}{H} + \frac{P^2}{H^2}\frac{j+1}{j}\right)$$

(S1d) $$\frac{dH}{dt} = (b_H - d_H)H - (\beta_P + \delta_P)P$$

Here, λ_P represents the *per capita* rate of parasite birth; $\mu_U(T)$ and $\mu_I(T)$ are the stage- and temperature-dependent *per capita* rates of parasite mortality; $\theta_U(T)$ is the temperature-dependent *per capita* development rate of uninfective parasite larvae to the infective stage; $\rho_H(T)H$ is the rate at which an infective larva encounters hosts (temperature-dependent for parasites that actively seek out host, and temperature-independent otherwise); q_H is the probability that a parasite establishes within its host following uptake; b_H and d_H are the rates of host birth and natural host death; β_P and δ_P quantify the effect of the parasite on host fecundity and death; and j describes the degree of parasite aggregation within the host population assuming a negative binomial distribution. Seasonal variability and potential range changes are ignored in this model for simplicity, but the model could easily be extended with these and other processes for more detailed analyses (Anderson & May, 1991; Keeling & Rohani, 2008).

$R_0(T)$, defined as the temperature-dependent expected lifetime reproductive output of a newborn larva in the absence of density-dependence (Anderson & May 1991), is then calculated as the dominant eigenvalue of the temperature-dependent next-generation matrix, $N(T)$, of equations S1 (Hurford et al., 2010). Here, $N(T) = F(T)V(T)^{-1}$ with

$$F(T)=\begin{pmatrix}0 & 0 & \lambda_P\\ 0 & 0 & 0\\ 0 & 0 & 0\end{pmatrix} \quad \text{and} \quad V(T)=\begin{pmatrix}\mu_U(T)+\theta_U(T) & 0 & 0\\ -\theta_U(T) & \mu_I(T)+\rho_H(T)H & 0\\ 0 & -q_H\rho_H(T)H & \mu_P+d_H+\delta_P\end{pmatrix},$$

from which we obtain

$$R_0(T)=\frac{q_H\lambda_P}{\mu_P+d_H+\delta_P}\cdot\frac{\theta_U(T)}{\mu_U(T)+\theta_U(T)}\cdot\frac{\rho_H(T)H}{\mu_I(T)+\rho_H(T)H} \quad .$$

Appendix S2. Why apparent development time is more temperature-sensitive than real development time

In this Appendix, we consider the development of uninfective free-living larvae to infectivity (Fig. 1B; stage L_U to L_I), and show that estimates of the activation energy of observed (apparent) development times, E_θ', will systematically overestimate the true activation energy of development, E_θ, due to a failure to account for the influence of mortality.

First, we note that the observed (apparent) distribution of development times will underestimate the actual distribution of development times in any cohort experiment if mortality is not accounted for (Braner & Hairston, 1989). More specifically, it can be shown that the difference between the true and apparent means of development time, M and M', equals the product of the variance in development time, σ^2, and the mortality rate, μ, if development times are normally distributed (Braner & Hairston, 1989) (Fig. S1A):

(S2) $$M - M' = \sigma^2 \mu \ .$$

As this difference increases with increasing temperatures (due to the temperature-dependence of the mortality rate, $\mu(T)$), estimates of E_θ' (apparent activation energy of development, based on $M'(T)$) will always overestimate the true activation energy of development E_θ (which needs to be estimated from the true development means, $M(T)$; Fig. S1B,C).

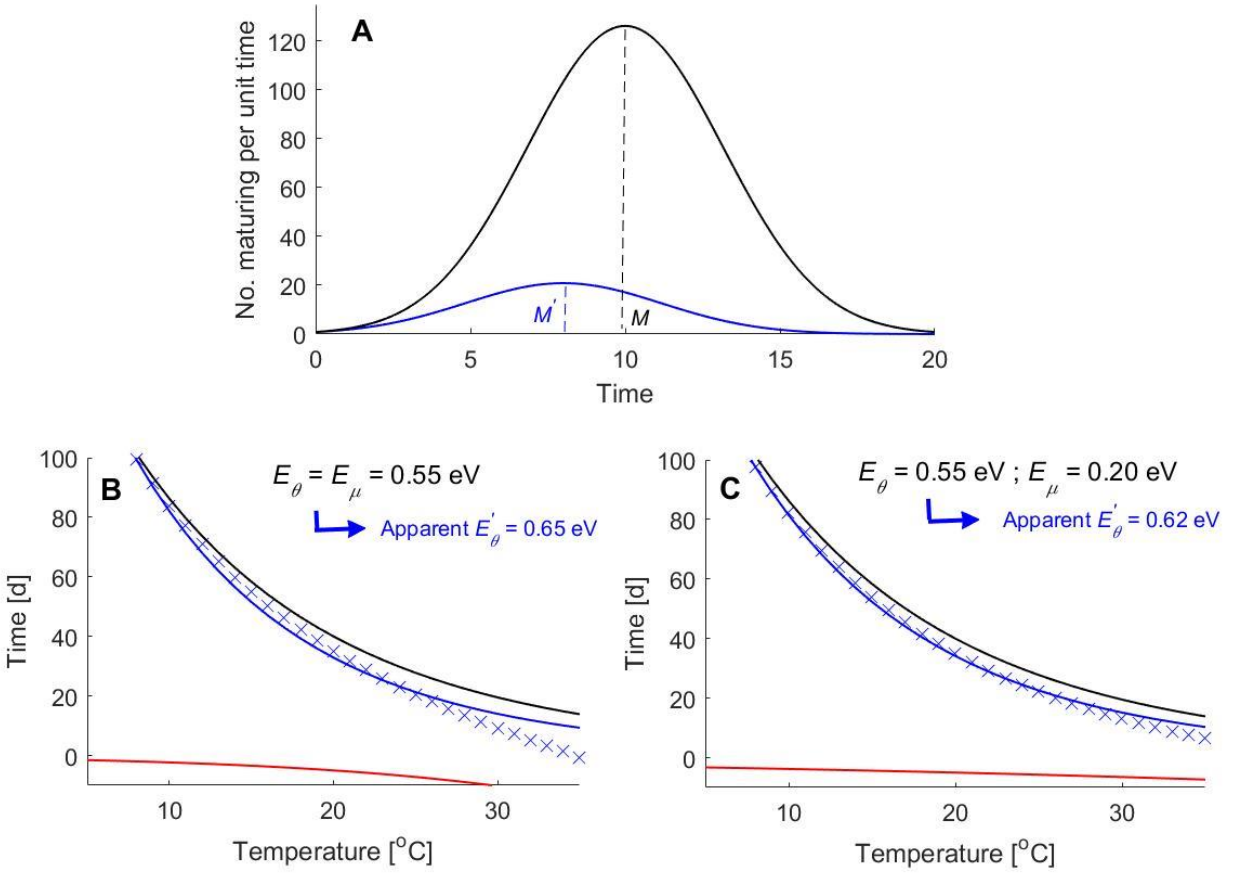

Figure S1. Why apparent development time is more temperature-sensitive than real development time. (A) The relationship between apparent and real development. Number of individuals maturing as a function of time when development time is normally distributed, without (=real development; black line) and with mortality (=apparent development; blue line). Vertical lines mark the mean development time without (M) and with ($M' = M - \sigma^2\mu$) mortality. Parameters were set as M = 10 d, σ^2 = 10 d^2 (variance of development time), and μ = 0.2 d^{-1} (mortality rate), implying M' = 8 d (eqn S2). Redrawn from Braner & Hairston (1989). Panels (B) and (C) illustrate why these discrepancies lead to biased (overestimated) activation energies of development time if these estimates are based on apparent development time. In both panels we assume that development time is normally distributed with a mean $M(T)$ that is temperature-sensitive according to the BA equation with activation energy E_θ = 0.55 eV, variance σ^2 = 10 d^2, and a baseline development time of $1/\theta_0$ = 40 d at T_0 = 20 C (black line). Furthermore, we assume that mortality rates also follow a BA equation with E_μ = 0.55 eV (panel B) or E_μ = 0.20 eV (panel C), and a baseline mortality of μ = 0.5 d^{-1} at T_0 = 20 C. Adding $-\sigma^2\mu(T)$ (red lines) to $M(T)$ yields apparent development times as a function of temperature, $M'(T)$ (eqn 5; blue crosses). Fitting a BA curve (eqn 1) to these simulated data (blue lines) yields activation energies E_θ' that overestimate the true activation energy of development E_θ, essentially because the contributions of mortality and developmental variance (red lines) lead to steeper temperature-dependencies in apparent development times (blue crosses) than in true development times (black line). This effect becomes stronger as mortality becomes more temperature-sensitive (contrast panels B & C; c.f. Fig. 5).

Appendix S3. The 'classical approach to perturbation analyses of $R_0(T)$ (Fig. S2), and R-codes for both the classical approach and the new approach suggested in Section 3.1

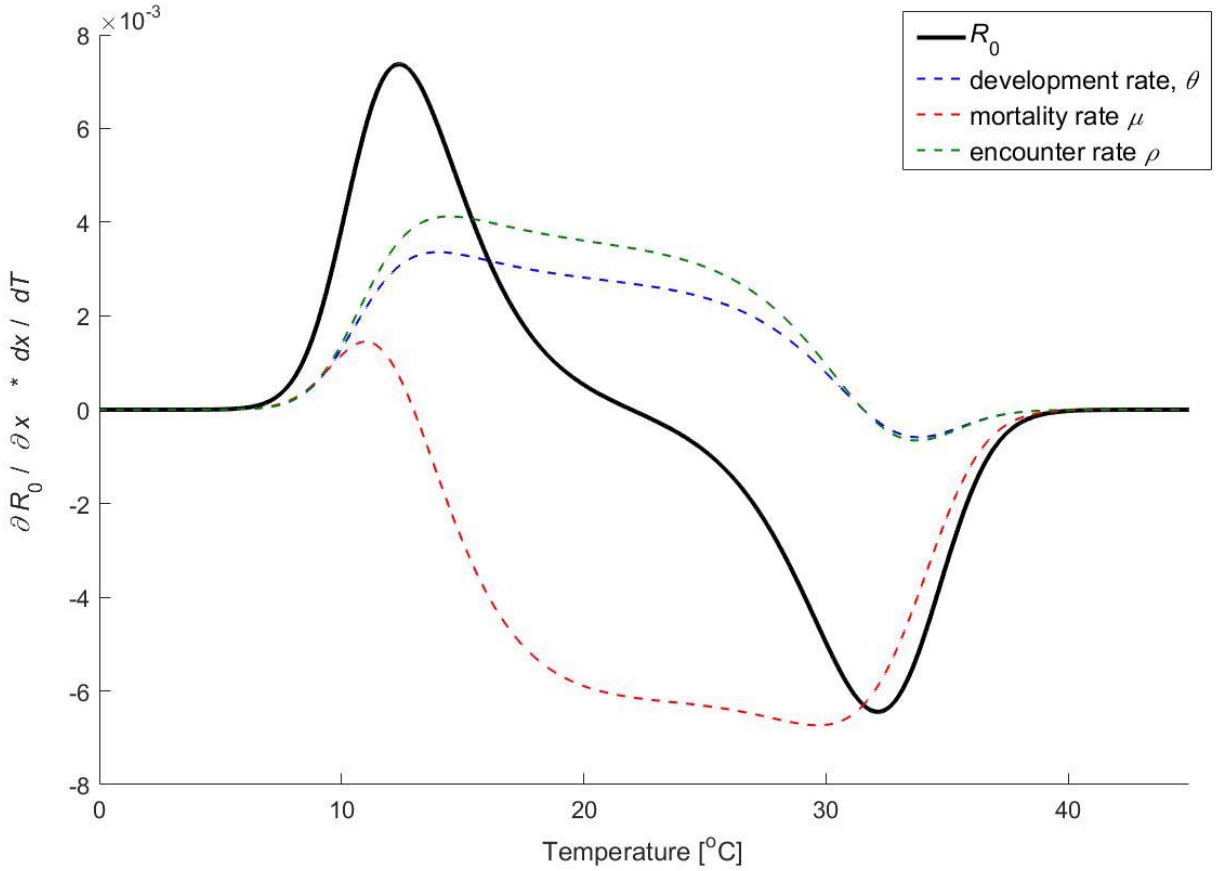

Figure S2. Perturbation analyses of an MTE-parameterized null model for a nematode with an endotherm host, a mandatory free-living stage, and active host infection (cf. Figs. 1, 3), but now using the 'classical approach' of determining the additive contributions of development (θ), mortality (μ), and host encounter (ρ) to the temperature sensitivity of $R_0(T)$, dR_0/dT. The additive contributions of each of these parameters are hereby calculated using the chain rule of partial derivatives, i.e. $dR_0/dT = \partial R_0/\partial\theta * d\theta/dT + \partial R_0/\partial\mu * d\mu/dT + \partial R_0/\partial\rho * d\rho/dT$. Black curve: sensitivity of $R_0(T)$ to temperature, dR_0/dT; blue (development), red (mortality), and green (encounter) curves show the additive contribution of each trait to this temperature-sensitivity (i.e. $\partial R_0/\partial x * dx/dT$). Baseline parameters of development (θ), mortality (μ) and encounter (ρ) rates are set as in Fig. 3: $\theta_0 = 0.03$ d^{-1}, $\mu_0 = 0.06$ d^{-1}, $\rho_0 = 0.01$ d^{-1} at $T_0 = 22.5$ C, and $E = 0.65$ eV, $-E^L = E^H = 3.25$ eV, $T^L = 10$ C, $T^H = 35$ C for all three traits.

S3.1 – R-code for the 'classical approach' to perturbation analyses of $R_0(T)$ (Fig. S2)

```
# The 'classical approach' to elasticity analyses of R0(T). This code
# reproduces Fig S2 of the article, that is, it decomposes the
# derivative of R0 w.r.t. temperature T, into its partial derivative
# w.r.t to the performance traits development, mortality, encounter
# rate, using the chain rule of partial derivations.

# Parameter settings ------------------------------------------------

minTemp <- 273.15   # setting min and max temperatures for simulations
maxTemp <- 318.15
resol <- 0.01
TT <-  seq(minTemp, maxTemp, resol)

theta0 <- 0.03; mu0 <- 0.06; rho0 <- 0.01      # baseline parameters
E_theta <- 0.65; E_mu <- 0.65; E_rho <- 0.65
T0_theta <- 295.65; T0_mu <- 295.65; T0_rho  <- 295.65
T0_thetaL <- 283.15; T0_muL <- 283.15; T0_rhoL <- 283.15
T0_thetaH <- 308.15; T0_muH <- 308.15; T0_rhoH <- 308.15
E_thetaL  <- -3.25; E_muL <- -3.25; E_rhoL <- -3.25;
E_thetaH <- 3.25; E_muH <- 3.25; E_rhoH  <- 3.25;
k <- 8.62*10^(-5)                              # Boltzmann's constant


# Sharpe-Schoolfield expressions for theta, mu, rho and Ro ----------

thetaSS <- quote(theta0 * exp(-(E_theta/k) * (1/T_ - 1/T0_theta)) *
(1+ exp(E_thetaL/k * (-1/T_+1/T0_thetaL)) + exp(E_thetaH/k *
(-1/T_+1/T0_thetaH)))^(-1))
muSS <-  quote(mu0    * exp(-(E_mu   /k) * (1/T_ - 1/T0_mu))    * (1+
exp(E_muL /k   * (-1/T_+1/T0_muL))    + exp(E_muH/k    *
(-1/T_+1/T0_muH))))
rhoSS <-  quote(rho0   * exp(-(E_rho  /k) * (1/T_ - 1/T0_rho))   * (1+
exp(E_rhoL/k   * (-1/T_+1/T0_rhoL))   + exp(E_rhoH/k   *
(-1/T_+1/T0_rhoH)))^(-1))

R0SS <- quote((rhoSS*thetaSS) / ((muSS + thetaSS) * (muSS + rhoSS)))

# Substitute the SS-models for theta, mu, rho into R0
R0SS <- substituteDirect(R0SS, list(thetaSS = thetaSS, muSS = muSS,
rhoSS = rhoSS))


# Derivatives of R0 and SS parameters with respect to temperature ----

dthetaSS_dT <- deriv(thetaSS, "T_")
dmuSS_dT <- deriv(muSS, "T_")
drhoSS_dT <- deriv(rhoSS, "T_")
dR0SS_dT <- deriv(R0SS, "T_")
```

```
# Create functions that evaluate the derivatives at given temperatures

f_dthetaSS_dT <- function(T) attr(eval(dthetaSS_dT, list(T_=T)),
"gradient")
f_dmuSS_dT <- function(T) attr(eval(dmuSS_dT, list(T_=T)), "gradient")
f_drhoSS_dT <- function(T) attr(eval(drhoSS_dT, list(T_=T)),
"gradient")
f_dR0SS_dT <- function(T) attr(eval(dR0SS_dT, list(T_=T)), "gradient")

# Derivatives of R0 with respect to the performance traits theta, mu,
# rho ------------------------

R0 <- quote((rho*theta)/((mu+theta)*(mu+rho)))

dR0_dtheta <- deriv(R0, "theta")
dR0_dmu <- deriv(R0, "mu")
dR0_drho <- deriv(R0, "rho")

# Substitute the SS-models for theta, mu and rho into the derivatives

dR0_dtheta <- substituteDirect(dR0_dtheta[[1]], list(theta = thetaSS,
mu = muSS, rho = rhoSS))
dR0_dmu <- substituteDirect(dR0_dmu[[1]], list(theta = thetaSS, mu =
muSS, rho = rhoSS))
dR0_drho <- substituteDirect(dR0_drho[[1]], list(theta = thetaSS, mu =
muSS, rho = rhoSS))

# Create functions that evaluate the derivatives at given temperatures

f_dR0_dtheta <- function(T) attr(eval(dR0_dtheta, list(T_=T)),
"gradient")
f_dR0_dmu <- function(T) attr(eval(dR0_dmu, list(T_=T)), "gradient")
f_dR0_drho <- function(T) attr(eval(dR0_drho, list(T_=T)), "gradient")

# Calculate the contributions of theta (development), mu (mortality),
# and rho (encounter rate) to dR0/dT

diffR0_dT <- f_dR0SS_dT(TT)
Cont_theta <- f_dR0_dtheta(TT)*f_dthetaSS_dT(TT)
Cont_mu <- f_dR0_dmu(TT)*f_dmuSS_dT(TT)
Cont_rho <- f_dR0_drho(TT)*f_drhoSS_dT(TT)
```

```
# Plotting the figures ------------------------------------------------
xticks <- seq(minTemp, maxTemp, 10)
xticklabels <- xticks-273.15
legendlabels <- c(expression(italic(R[0])),
                  expression(paste("development rate ", theta, sep =
""")),
                  expression(paste("mortality rate ", mu, sep = "")),
                  expression(paste("encounter rate ", rho, sep = "")))
cols <- c("black", "blue", "red", "green")

curve(f_dR0SS_dT(x), minTemp, maxTemp, xlab = "", ylab = "", xaxt =
"n", col = cols[1])
curve(f_dR0_dtheta(x)*f_dthetaSS_dT(x), minTemp, maxTemp, lty=2,
col=cols[2], add=T)
curve(f_dR0_dmu(x)*f_dmuSS_dT(x), minTemp, maxTemp, lty=2,
col=cols[3], add=T)
curve(f_dR0_drho(x)*f_drhoSS_dT(x), minTemp, maxTemp, lty=2,
col=cols[4], add=T)

axis(1, at = xticks, labels = xticklabels)
title(xlab = "Temperature (˚C)",
      ylab =
expression(partialdiff*italic(R[0])/partialdiff*italic(x)%*%italic(d*x
)/italic(d*T)))
legend("topright", legend = legendlabels, col = cols, lty =
c(1,2,2,2), cex = 0.75)
```

S3.2 – R-code for the perturbation analyses approach of $R_0(T)$ suggested in Section 3.1 (Fig. 6)

```
# Elasticity analyses of R0(T) with respect to the two metrics (AUC,
# skewness) in section 3.1. This code reproduces Figure 6 of the
# article, that is, it calculates the relative change in the area
# under the curve and skewness of R_0(T) for a proportional change in
# the activation energies, inactivation energies, and baseline
# performance values of the Sharpe-Schoolfield models for the
# performance traits that underlie R0(T).

# Parameter settings ------------------------------------------------

minTemp <- 273.15   # setting min and max temperatures for simulations
maxTemp <- 318.15
resol <- 0.01
TT <-  seq(minTemp, maxTemp, resol)         # temperature vector for
                                            # calculations

theta0 <- 0.03; mu0 <- 0.06; rho0 <- 0.01      # baseline parameters
E_theta <- 0.65; E_mu <- 0.65; E_rho <- 0.65
T0_theta <- 295.65; T0_mu <- 295.65; T0_rho  <- 295.65
T0_thetaL <- 283.15; T0_muL <- 283.15; T0_rhoL <- 283.15
T0_thetaH <- 308.15; T0_muH <- 308.15; T0_rhoH <- 308.15
E_thetaL  <- -3.25; E_muL <- -3.25; E_rhoL <- -3.25;
E_thetaH <- 3.25; E_muH <- 3.25; E_rhoH  <- 3.25;
k <- 8.62*10^(-5)                              # Boltzmann's constant

# Create the elasticity matrices. The number of columns corresponds
# to the number of parameters, and the number of rows is the number
# of relative differences to be tested (here, 0%, -20%, +20%)

Elast_Skew <- matrix(0, nrow = 3, ncol = 12)
Elast_AUC <- matrix(0, nrow = 3, ncol = 12)

# Set a vector containing the original parameter values

Base_Params_Orig <- c(theta0, E_theta, E_thetaL, E_thetaH, mu0, E_mu,
E_muL, E_muH, rho0, E_rho, E_rhoL, E_rhoH)

# Define the vector of relative differences in parameter values that
# will be tested

Perc_change <- c(1, 0.8, 1.2)
```

```
# Definition of SS-models for development (theta), mortality (mu),
# encounter rate (rho), and the resulting R0(T) (cf. eqn 3; the
# temperature-independent constant C is ignored as it cancels out in
# the elasticity analyses)----------------------------

R0_fun <- function(Temp, Pars) {
  theta_SS <- Pars[1] * exp(-Pars[2]/k * (1/Temp-1/T0_theta)) *
(1+exp(Pars[3]/k * (-1/Temp+1/T0_thetaL)) + exp(Pars[4]/k *
(-1/Temp+1/T0_thetaH)))^(-1)
  mu_SS <- Pars[5] * exp(-(Pars[6]/k) * (1/Temp - 1/T0_mu)) *
(1+ exp(Pars[7]/k * (-1/Temp+1/T0_muL))   + exp(Pars[8]/k *
(-1/Temp+1/T0_muH)))
  rho_SS <-  Pars[9] * exp(-(Pars[10]/k) * (1/Temp - 1/T0_rho)) *
(1+ exp(Pars[11]/k * (-1/Temp+1/T0_rhoL)) +  exp(Pars[12]/k *
(-1/Temp+1/T0_rhoH)))^(-1)

  R0_SS <- theta_SS/(mu_SS + theta_SS)*rho_SS/(mu_SS+rho_SS)
  return(R0_SS)
}

# Calculating the relative changes in R_0 for each parameter variation

for (i in 1:length(Base_Params_Orig)) {
  for (j in 1:length(Perc_change)) {
    Base_Params <- Base_Params_Orig

    # Change parameter i in the parameters vector
    Base_Params[i] <- Base_Params[i]*Perc_change[j]

    # Calculate the new R_0 for all temperatures
    R0_SS <- R0_fun(TT, Base_Params)

    # Determine at which temperature the maximum R0 is reached
    max_index <- which.max(R0_SS)
    T_pk <- TT[max_index]

    # Calculate the value of the 2 objective functions (skewness, AUC)
    skew = (T_pk-T0_thetaL)/(T0_thetaH-T0_thetaL)
    AUC1 = integrate(R0_fun, minTemp, maxTemp, Pars =
      Base_Params)$value

    if (j == 1) {
      Elast_Skew[j, i] <- skew
      Elast_AUC[j, i] <- AUC1
    } else {
      Elast_Skew[j, i] <- skew/Elast_Skew[1, i]-1
      Elast_AUC[j, i] <- AUC1/Elast_AUC[1, i]-1
    }
  }
}
```

```
# Plotting the Figures ------------------------------------------------

# Create a matrix for each of the second and third row in the
# elasticity matrices. This is needed for the barplots.
EA1 <- t(array(Elast_AUC[2,],c(4,3)))
EA2 <- t(array(Elast_AUC[3,],c(4,3)))
ES1 <- t(array(Elast_Skew[2,],c(4,3)))
ES2 <- t(array(Elast_Skew[3,],c(4,3)))

AUC_yrange <- c(min(EA1, EA2), max(EA1, EA2))
Skew_yrange <- c(min(ES1, ES2), max(ES1, ES2))
Par_labels <- expression(italic(y[0]),
                         italic(E),
                         italic(E[L]),
                         italic(E[H]))
legendlabels <- expression(paste("development rate ", theta, sep =
""),
                           paste("mortality rate ", mu, sep = ""),
                           paste("encounter rate ", rho, sep = ""))
plotcolors <- topo.colors(3)

barplot(EA1, ylim = AUC_yrange , names.arg = Par_labels, beside = T,
col = plotcolors, ylab = "Relative change in AUC")
barplot(EA2, beside = T, add=T, col = plotcolors, density = 15)
legend("topright", legend = legendlabels, fill = plotcolors, cex =
0.75)

barplot(ES1, ylim = Skew_yrange, names.arg = Par_labels, beside = T,
col = plotcolors, ylab = "Relative change in Skewness")
barplot(ES2, beside = T, add=T, col = plotcolors, density = 15)
legend("topright", legend = legendlabels, fill = plotcolors, cex =
0.75)
```

Appendix S4. Case study in SS model fitting using *Schistosoma mansoni* cercaria activity data

Here, we provide a detailed case study showing how to fit the SS model to thermal performance data (here, cercaria swimming speed), following the maximum likelihood approach of Régnière et al. (2012) and implementing it in R (R Development Core Team, 2014).

S4.1 – Study species

The trematode parasite *Schistosoma mansoni* is the most widespread parasitic agent of human schistosomiasis (Colley et al., 2014). The parasite has a two-host life cycle, where free-swimming cercariae seek out humans after being released from the intermediate host snail *Biomphalaria glabrata* (Colley et al., 2014) (Fig. 1C, D). We conducted an experiment to quantify the temperature dependence of *S. mansoni* cercaria swimming speed as a proxy for parasite metabolism. The methods for data collection are provided in Section S4.2, and the data fitting procedures are detailed in the subsequent sections.

S4.2 – Experimental design and data collection

S. mansoni-infected *B. glabrata* snails were obtained from the Schistosomiasis Resource Center (BEI Resources, NIAID, NIH). Snails were maintained at room temperature (22 C) in artificial spring water (Cohen et al., 1980) with a 12:12 hour photoperiod, Snails were fed *ad libitum* a combination of frozen spinach and "snail jello", which is an agar preparation that includes calcium powder and ground Tetramin™ fish flakes (Paull et al., 2015). Prior to cercaria collection, five infected snails were moved to a temperature-controlled Styrofoam incubator (Raffel et al., 2013) and were maintained there at 22 C for one week. Two days prior to the experiment (day 6 of acclimation), a wooden panel was placed over the clear lid of the incubator to maintain complete darkness (0:24 photoperiod) for the remaining 2 days. Snails were then placed under a bright LED light for 1 hour to encourage cercaria release. *S. mansoni* cercariae were collected and fluorescently stained with a fluorescently-labeled fatty acid analogue (BODIPY FL C12; Invitrogen, Carlsbad, CA, USA) following the protocol of LaFonte et al. (2015). The experiment was conducted in two temporal blocks. All cercariae were observed within 3 hours of release from the snail (n=49). The order in which cercariae were exposed to temperature treatments was randomized within temporal blocks to account for potential changes in cercariae viability throughout the day.

Individual cercaria were then pipetted into the depression on the underside of a specimen cup with approximately 5 µL of 22 C artificial spring water (Fig. S3). The lid was then floated for five minutes in 250 mL of water, maintained at one of eight temperatures (13, 16, 19, 22, 25, 28, 31, 34 C) to ensure that the water in the depression containing the cercaria had reached and stayed at the target temperature. We verified that this timing was sufficient using an infrared thermometer prior to the experiment. Each cercaria was viewed under a fluorescent stereomicroscope (Leica MZ10F, Leica Microsystems, Wetzler, Germany) fitted with a color digital video camera (Leica DFC450C, Leica Microsystems, Wetzler, Germany). Video recordings of cercaria activity were obtained using the MicroManager software (Edelstein et al., 2014) interacting with VirtualDub screen capture software (www.virtualdub.org). Cercaria swimming speed was quantified by tracking the position of each cercaria's tail base throughout each video and calculating the velocity between successive points in millimeters per second ($mm \cdot sec^{-1}$).

S4.3 – Loading and plotting data

The following code loads the experimental data (performance temperature, cercaria swimming speeds, temporal block) into the R console and creates a dataframe named "myData".

```
#Experimental performance temperatures (°C)
PerfTemp <- c(22, 22, 19, 19, 22, 19, 25, 13, 13, 25, 25, 16, 31, 16, 16, 31,
     31, 34, 34, 28, 28, 28, 34, 34, 34, 28, 34, 28, 34, 34, 28, 31, 16, 31,
     16, 16, 31, 19, 19, 22, 22, 19, 25, 13, 13, 25, 13, 13, 25)

#Cercaria swimming speeds (mm/sec)
Velocity <- c(0.833, 0.209, 0.201, 0.115, 0.183, 0.143, 0.611, 0.165,
     0.199, 0.597, 0.416, 0.097, 0.208, 0.292, 0.159, 0.370, 0.228, 0.152,
     0.178, 0.502, 0.516, 0.480, 0.270, 0.191, 0.255, 0.508, 0.248, 0.585,
     0.215, 0.115, 0.601, 0.165, 0.181, 0.268, 0.289, 0.122, 0.241, 0.173,
     0.194, 0.180, 0.369, 0.406, 0.281, 0.198, 0.302, 0.449, 0.208, 0.052,
     0.417)

#Temporal blocks in the experiment
#Random effects must be entered as numeric vectors for this model formulation
BlockReal <- c(1, 1, 1, 1, 1, 1, 1, 1, 1, 1, 1, 1, 1, 1, 1, 1, 1, 1, 1, 1, 1,
     1, 1, 1, 2, 2, 2, 2, 2, 2, 2, 2, 2, 2, 2, 2, 2, 2, 2, 2, 2, 2, 2, 2, 2,
     2, 2, 2, 2)

myData <- as.data.frame(cbind(PerfTemp,Velocity))
myData$PerfTemp <- as.double(PerfTemp)       #numeric variable
myData$Velocity <- as.double(Velocity)       #numeric variable
```

These data can now be plotted using

```
plot(PerfTemp,Velocity)
```

Note that the data clearly extend beyond T_{pk}, capturing the high-temperature inactivation (Fig. 7B). We therefore proceed with fitting the SS model to these thermal performance data, and not the simpler BA-model, which is unable of capturing these nonlinearities.

S4.4 – Fitting the Sharpe-Schoolfield (SS) model to thermal performance data using maximum likelihood

Our dataset did not include temperatures close enough to the critical thermal minimum of *S. mansoni*, so we could not estimate the low-temperature inactivation energy (E^L) or the corresponding threshold (T^L). We therefore simplified the SS model by omitting these terms (i.e. setting T^L=0 K) and describe the temperature-dependence of cercaria performance $p(T)$ within the experimental temperature range using

$$\text{(S3)} \qquad p(T) = p_0 e^{-\frac{E}{k}\left(\frac{1}{T}-\frac{1}{T_0}\right)} \cdot \left[1 + e^{\frac{E^H}{k}\left(\frac{1}{T^H}-\frac{1}{T}\right)}\right]^{-1}.$$

The following code implements the maximum likelihood approach of Régnière et al. (2012) in R, estimating the activation energy (E), high-temperature inactivation energy (E^H) and temperature threshold (T^H) of cercaria swimming speed.

```
#Define constants
k  <- 8.62*10^(-5)      #Boltzmann's constant
K  <- 273.15            #Celsius to Kelvin conversion
To <- 19 + K            #Standardization temperature

#Log-likelihood function to be optimized, assuming a log-normal error
#distribution (after Régnière et al., 2012)

SSmodel <- function(data, par){
   s_epsilon <- par[1]
   pTo <- par[2]
   E   <- par[3]
   Th  <- par[4]
   Eh  <- par[5]

   se2 <- (-0.5)*s_epsilon^2  #mean of the normally distributed variable
                              #'epsilon' below (Régnière et al., 2012)
   x <- data[,1]+K
   y <- data[,2]

   expected <- pTo*exp(-(E/k*(1/x-1/To)))*(1+exp(Eh/k*(1/Th-1/x)))^-1
   epsilon <- log(y/expected)       #note that errors are calculated as
                                    #ratios, not differences

   p <- dnorm(epsilon,se2,s_epsilon)

   for (i in 1:length(p)){
      if(p[i] < 1e-10) p[i] <- 1e-10     #prevents log(0) computation errors
   }

   LL<- sum(log(p))
   -LL
}

#'Reasonable' initial parameter estimates to ensure convergence of the
#optimization procedure
init <- c(s_epsilon= 0.1, pTo= 0.2, E= 0.65, Th= 303, Eh= 3.5)


#Set parameter lower and upper parameter boundaries
lower <- c(0, 0, 0, 0, 0)
upper <- c(Inf, Inf, Inf, Inf, Inf)

#Optimize full model for all parameters
model <- optim(par= init, fn= SSmodel, data= myData,
   method= "L-BFGS-B", lower= lower, upper= upper, hessian=TRUE)
model                                    #view model output

#Output optimized model coefficients and their 95% confidence intervals
Coef <- model$par
SE <- sqrt(diag(solve(model$hessian)))    #SE for parameter estimates
Value <- SE*1.96               #95% confidence intervals for estimates
```

```
cbind(Coef, Value)

#Table of model parameter estimates and the value to calculate 95% confidence
#intervals (Coef +/- Value)
#                 Coef      Value
#s_epsilon   0.4197777 0.08310917
#pTo         0.2703667 0.04715787
#E           0.6984673 0.29862724
#Th        303.4948870 2.91925910
#Eh          3.2046242 1.32339403

#Plot the optimized model function over data (Fig. 7B, solid black line).
plot(PerfTemp, Velocity)             #plot data
cercSwim <- function(x, pTo, E, Eh, Th){
   y = pTo*exp(-(E/k*(1/x-1/To)))*(1+exp(Eh/k*(1/Th-1/x)))^-1
}
LineTemps <- seq(13, 34, length= 100) + K
PredictionsDnorm <- cercSwim(x= LineTemps, pTo= 0.270 , E= 0.698 , Eh= 3.205
, Th= 303.5)
lines(LineTemps-K, PredictionsDnorm)   #plot optimized SS model
```

The optimized parameter values of the SS-model and their confidence intervals are provided in the table above, and the model fit to data is shown in Fig. 7B. Our parameter estimates conformed closely to *a priori* expectations based on the interspecific means of activation energies (E = 0.65 eV; Gillooly et al., 2001; Brown et al., 2004) and inactivation energies (E^H = 5 × 0.65 eV = 3.25 eV; Molnár et al., 2013), although we note that this need not be the case in general (Section 2). However, our estimate of the high-temperature inactivation threshold T^H = 303.49 ± 2.92 K (= 30.34 ± 2.92 C) for cercaria swimming speed was nearly 15 C lower than the literature estimate of CT_{max} = 45 C for *S. mansoni* (Lawson & Wilson, 1980). This is probably because our measure of parasite performance differed from that assessed by Lawson and Wilson (1980), who measured the temperature needed to induce 100% cercaria mortality. Schistosome cercariae use temperature as one way of detecting definitive hosts, and they might interpret environmental temperatures similar to that of their definitive host's body temperature (37 C) as an indication that a definitive host is nearby (Colley et al., 2014). For this reason, temperatures greater than 37 C might induce a behavioral response in which cercariae stop swimming and shed their tails in preparation to penetrate a definitive host (Colley et al., 2014). Indeed, during this experiment we frequently observed *S. mansoni* cercariae that stopped swimming and began crawling along the cup surface in the high temperature treatments (31 and 34 C), supporting this interpretation.

S4.5 – Adding a random effect to the SS model with log-normal error structure

In this final section, we modify the R code from Section S4.4 to allow for the addition of potential random effects in the sampling design. Such random effects may, for example, arise when experiments are conducted on individuals originating from separate source populations, when individuals have differing thermal histories, or when experiments are conducted in multiple temporal blocks or incubators. Régnière *et al.* (2012) showed how to incorporate a random effect into the likelihood function of the SS model, and provide example SAS code. The primary change to the previous code is the addition of a new parameter, `s_upsilon`, which represents the

standard deviation of the population means. For example, in an experiment with multiple blocks, this parameter would describe the standard deviation of the block means.

Our experiment with *S. mansoni* cercariae was conducted in 2 temporal blocks (cf. variable `BlockReal` in S4.3). However, model optimization showed that the random effect of block was negligible (`s_upsilon` < 0.0001) in our data[1]. A block effect so small is difficult to evaluate statistically and can make the model unstable, because the likelihood function approaches infinity as `s_upsilon` approaches zero. We therefore created an artificial blocking variable `BlockFake`) for demonstration purposes, where each data point was assigned to `BlockFake` = 1 if swimming speed was lower than the mean swimming speed at that performance temperature, and to `BlockFake` = 2 if it was higher (Figure S4).

```
#Artificial (fake) blocking variable for demonstration purposes

BlockFake <- c(2, 1, 1, 1, 1, 1, 2, 1, 2, 2, 1, 1, 1, 2, 1, 2, 1, 1, 1, 1, 1,
1, 2, 1, 2, 1, 2, 2, 2, 1, 2, 1, 1, 2, 2, 1, 1, 1, 1, 1, 2, 2, 1, 2, 2, 1, 2,
1, 1)

myData2 <- as.data.frame(cbind(PerfTemp,Velocity,BlockFake))
myData2$PerfTemp <- as.double(PerfTemp)         #numeric
myData2$Velocity <- as.double(Velocity)         #numeric

#Modified maximum likelihood approach, including a random effect:

#define constants
k <- 8.62*10^(-5)     #Boltzmann's constant (eV/K)
K <- 273.15           #Celsius to Kelvin conversion
To <- 19 + K          #Standardization temperature (arbitrary)

SSmodelrandom <- function(data, par){
  s_epsilon <- par[1]
  s_upsilon <- par[2]
  pTo <- par[3]
  E  <- par[4]
  Th <- par[5]
  Eh <- par[6]
```

[1] Optimizing this model with the real temporal block variable (BlockReal) required precise selection of initial parameter estimates and a more forgiving optimization method to achieve model convergence, due to the negligibly small magnitude of the random effect (s_upsilon ≈ 2.0×10^{-9}). The traditional "optim" function only has one available method for bounded parameter optimization ("L-BFGS-B"). To estimate s_upsilon for the BlockReal effect, we used the updated "optimx" function (package optimx) which allows bounded parameter estimation using the robust "spg" method (Nash & Varadhan, 2011; Nash, 2014). Such a small s_upsilon is problematic because the likelihood function approaches infinity as s_upsilon approaches zero (Régnière et al., 2012), leading to inflated likelihood values and thus potentially inaccurate estimates for other parameters. It is often easier to achieve model convergence with a simpler model (in this case, the earlier model with no random effect), and this can be a good way to refine starting values for more complex models that might have more trouble converging. In this case, plotting the data also helped to reveal the negligible difference between blocks, leading us to try out the smaller starting values for s_upsilon that ultimately led to model convergence.

```
  se2 <- (-0.5)*s_epsilon^2

  x <- data[,1]+K; y <- data[,2]; Block <- data[,3]

  expected <- pTo*exp(-(E/k*(1/x-1/To)))*(1+exp(Eh/k*(1/Th-1/x)))^-1
  data <- cbind(data, expected)
  upsilon <- numeric(length(x))

  for (j in 1:max(Block)){
    #upsilon_j is the mean deviation from expected for treatment j
    upsilon_j <- mean(subset(data, Block==j)[,2]/subset(data,
                 Block==j)[,4])
    #insert each datapoint's upsilon value into the dataframe
      for (i in 1:length(x)){
        if (Block[i]==j) upsilon[i] <- upsilon_j
      }
  }
  epsilon <- log(y/(expected*upsilon))      #See Régnière et al. 2012

  if(s_upsilon < 1e-20) s_upsilon <- 1e-20  #helps prevent NaN's
  if(s_epsilon < 1e-5) s_epsilon <- 1e-5

  p1 <- dnorm(upsilon, mean= 1, sd= s_upsilon)
  p2 <- dnorm(epsilon, mean= se2, sd= s_epsilon)

  for (i in 1:length(p1)){                  #helps prevent NaN's
    if(p1[i] < 1e-5) p1[i] <- 1e-5
    if(p2[i] < 1e-5) p2[i] <- 1e-5
  }

  LL <- sum(log(p1*p2))
  return(-LL)
}

#Initial parameter estimates and boundaries for parameter search space
init <- c(s_epsilon= 0.4, s_upsilon= 0.5, pTo= 0.2704665,
            E= 0.697644, Th= 303, Eh= 3.2059197)

lower <- c(0, 0, 0, 0, 0, 0)
upper <- c(Inf, Inf, Inf, Inf, Inf, Inf)

#Optimize full model for all parameters
model <- optim(par= init, fn= SSmodelrandom, data= myData2,
         method= "L-BFGS-B", lower= lower, upper= upper, hessian=TRUE)
model

#Output optimized model coefficients and their standard errors
coef <- model$par
SE <- sqrt(diag(solve(model$hessian)))   #SE for parameter estimates
Value <- SE*1.96                         #95% confidence intervals
cbind(coef,Value)
```

```
#Table of model parameter estimates and the value to calculate 95% confidence
#intervals (Coef +/- Value)
#                 coef       Value
# s_epsilon   0.2923503 0.05986718
# s_upsilon   0.2872339 0.05993339
# pTo         0.3010968 0.03805723
# E           0.6950091 0.22658316
# Th        303.2161098 2.26526098
# Eh          3.0731122 0.91245373


#Plot model
#subset the blocks
blockL <- subset(myData2,BlockFake=="1")
blockH <- subset(myData2,BlockFake=="2")
plot(blockH$PerfTemp,blockH$Velocity,
  pch=1,col='red',ylim=c(0,1), , bty="l",
  xlab="Temperature (C)", ylab="Cercaria swimming speed (mm/sec)")
points(blockL$PerfTemp,blockL$Velocity,pch=16,col='blue')

LineTemps<-seq(13,35,length=100)+K
Predictions<-cercSwim(x=LineTemps, pTo= 0.301 , E= 0.695 , Eh= 3.073 , Th=
303.216)          #full model predictions
PredictionsHigh<-Predictions+(Predictions*.287)       #high block predictions
PredictionsLow<-Predictions-(Predictions*.287)        #low block predictions
lines(LineTemps-K, PredictionsHigh, lwd=2, lty=3,col='red')
lines(LineTemps-K, PredictionsLow,lwd=2, lty=2,col='blue')
```

Including this artificial (fake) random effect, maximum likelihood estimated `s_epsilon` = 0.292 ± 0.060 mm·sec^{-1} and `s_upsilon` = 0.287 ± 0.060 mm·sec^{-1}, showing that the block effect accounted for about half of the random error in this dataset as expected. The remaining parameter estimates were similar to those obtained without a random effect (p_0 = 0.301 ± 0.038 mm·sec^{-1}; E = 0.695 ± 0.227 eV; T^H = 303.22 ± 2.27 K [= 30.07 ± 2.27 C]; E^H = 3.073 ± 0. 912 eV).

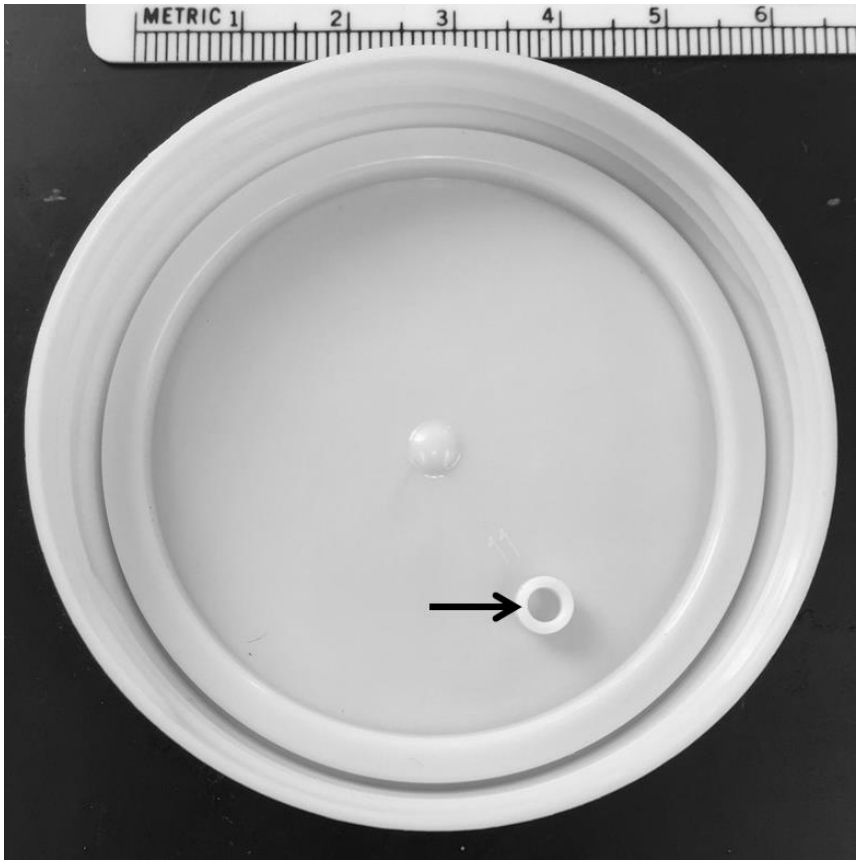

Figure S3. Photograph of the specimen cup lids used in the cercaria swimming speed experiment. Arrow indicates the depression used to contain individual cercaria during video capture. Metric ruler included for scale.

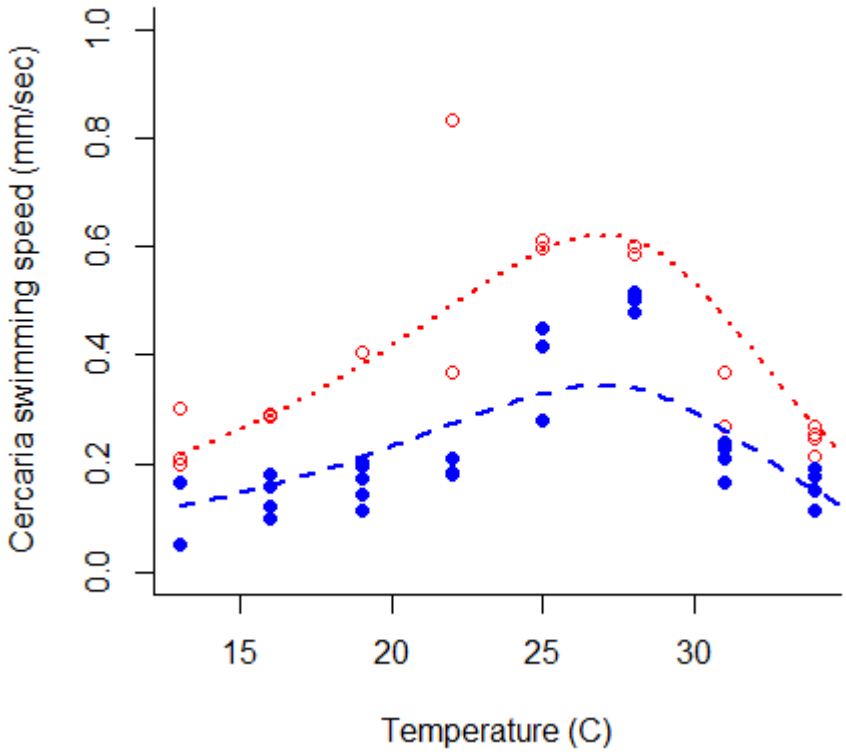

Figure S4. Visualization of the artificially created (fake) block effect on the *S. mansoni* cercariae swimming speed experimental data. Blue, closed circles represent swimming speeds below the mean swimming speed at that temperature (Block 1), and red, open circles represent swimming speed above the mean speed at that temperature (Block 2). The best-fitting SS-model that accounts for this block effect (Block 1: blue dashed curve; Block 2: red dotted curve) was estimated using the code in S4.5.

Literature Cited for Supporting Information:

Anderson, R. M. and R. M. May. 1978. Regulation and stability of host-parasite population interactions: I. Regulatory processes. Journal of Animal Ecology **47:** 219-247.

Anderson, R. M. and R. M. May. 1991. Infectious diseases of humans: Dynamics and control. Oxford Science Publications, Great Britain, 757 p.

Braner, M. and N. G. Hairston. 1989. From cohort data to life table parameters via stochastic modeling. *In* Estimation and analysis of insect populations, L. L. McDonald, B. F. J. Manly, J. A. Lockwood, and J. A. Logan (eds.). Springer-Verlag, Berlin, p. 81-92.

Brown, J. H., J. F. Gillooly, A. P. Allen, V. M. Savage and G. B. West. 2004. Toward a metabolic theory of ecology. Ecology **85:** 1771-1789.

Cohen, L. N., H. Neimark and L. K. Eveland. 1980. *Schistosoma mansoni*: response of cercariae to a thermal gradient. Journal of Parasitology **66:** 362-364.

Colley, D. G., A. L. Bustinduy, E. Secor and C. H. King. 2014. Human schistosomiasis. Lancet **383:** 2253-2264.

Edelstein, A. D., M. A. Tsuchida, N. Amodaj, H. Pinkard, R. D. Vale and N. Stuurman. 2014. Advanced methods of microscope control using μManager software. Journal of Biological Methods **1:** e11.

Gillooly, J. F., J. H. Brown, G. B. West, V. M. Savage and E. L. Charnov. 2001. Effects of size and temperature on metabolic rate. Science **293:** 2248-2251.

Hurford, A., D. Cownden and T. Day. 2010. Next-generation tools for evolutionary invasion analyses. Journal of the Royal Society Interface **7:** 561-571.

Keeling, M. J. and P. Rohani. 2008. Modeling infectious diseases in humans and animals. Princeton University Press, Princeton, N.J., 366 p.

LaFonte, B. E., T. R. Raffel, I. N. Monk and P. T. J. Johnson. 2015. Quantifying larval trematode infections in hosts: A comparison of method validity and implications for infection success. Experimental Parasitology **154:** 155-162.

Lawson, J. R. and R. A. Wilson. 1980. The survival of the cercariae of *Schistosoma mansoni* in relation to water temperature and glycogen utilization. Parasitology **81:** 337-348.

Molnár, P. K., S. J. Kutz, B. M. Hoar and A. P. Dobson. 2013. Metabolic approaches to understanding climate change impacts on seasonal host-macroparasite dynamics. Ecology Letters **16:** 9-21.

Nash, J. C. 2014. On best practice optimization methods in R. Journal of Statistical Software **60:** 1-14.

Nash, J. C. and R. Varadhan. 2011. Unifying optimization algorithms to aid software system users: optimx for R. Journal of Statistical Software **43:** 1-14.

Paull, S. H., T. R. Raffel, B. E. LaFonte and P. T. J. Johnson. 2015. How temperature shifts affect parasite production: testing the roles of thermal stress and acclimation. Functional Ecology **29:** 941-950.

R Development Core Team. 2014. R: A language and environment for statistical computing. R Foundation for Statistical Computing, Vienna, Austria.

Raffel, T. R., J. M. Romansic, N. T. Halstead, T. A. McMahon, M. D. Venesky and J. R. Rohr. 2013. Disease and thermal acclimation in a more variable and unpredictable climate. Nature Climate Change **3:** 146-151.

Régnière, J., J. Powell, B. Bentz and V. Nealis. 2012. Effects of temperature on development, survival and reproduction of insects: Experimental design, data analysis and modeling. Journal of Insect Physiology **58:** 634-647.